

# Proposal for U.S. participation in Double-CHOOZ: A New $\theta_{13}$ Experiment at the Chooz Reactor

S. Berridge<sup>g</sup>, W. Bugg<sup>g</sup>, J. Busenitz<sup>a</sup>, S. Dazeley<sup>e</sup>,  
G. Drake<sup>b</sup>, Y.Efremenko<sup>g</sup>, M. Goodman<sup>b\*</sup>, J. Grudzinski<sup>b</sup>,  
V. Guarino<sup>b</sup>, G. Horton-Smith<sup>d</sup>, Y. Kamyshev<sup>g</sup>, T. Kutter<sup>e</sup>  
C. Lane<sup>c</sup>, J. LoSecco<sup>f</sup>, R. McNeil<sup>e</sup>, W. Metcalf<sup>e</sup>,  
D. Reyna<sup>b</sup>, I. Stancu<sup>a</sup>, R. Svoboda<sup>e\*</sup>, R. Talaga<sup>b</sup>

October 14, 2004

<sup>a</sup> University of Alabama, <sup>b</sup> Argonne National Laboratory, <sup>c</sup> Drexel University,  
<sup>d</sup> Kansas State University, <sup>e</sup> Louisiana State University,  
<sup>f</sup> University of Notre Dame, <sup>g</sup> University of Tennessee  
\* US Contacts: phsvob@lsu.edu, maury.goodman@anl.gov

## Abstract

It has recently been widely recognized that a reactor anti-neutrino disappearance experiment with two or more detectors is one of the most cost-effective ways to extend our reach in sensitivity for the neutrino mixing angle  $\theta_{13}$  without ambiguities from CP violation and matter effects[1]. The physics capabilities of a new reactor experiment together with superbeams and neutrino factories have also been studied [2, 3] but these latter are considered by many to be more ambitious projects due to their higher costs, and hence to be farther in the future.

We propose to contribute to an international collaboration to modify the existing neutrino physics facility at the Chooz-B Nuclear Power Station in France. The experiment, known as Double-CHOOZ, is expected to reach a sensitivity of  $\sin^2 2\theta_{13} > 0.03$  over a three year run, 2008-2011. This would cover roughly 85% of the remaining allowed region. The costs and time to first results for this critical parameter can be minimized since our project takes advantage of an existing infrastructure.

# Contents

<b>1</b>	<b>Description of the Double-CHOOZ Experiment</b>	<b>1</b>
1.1	Introduction . . . . .	1
1.2	Physics Motivation . . . . .	1
1.2.1	$\bar{\nu}_e$ detection principle . . . . .	2
1.2.2	$\bar{\nu}_e$ oscillations . . . . .	2
1.3	Configuration of the Detectors for Double-CHOOZ . . . . .	3
1.3.1	The CHOOZ nuclear reactors . . . . .	3
1.3.2	Detector design . . . . .	5
1.4	Scintillator . . . . .	10
1.4.1	Liquid inventory . . . . .	10
1.4.2	Scintillator fluid systems . . . . .	10
1.5	Calibration . . . . .	11
1.6	Background . . . . .	13
1.6.1	Intrinsic backgrounds . . . . .	14
1.6.2	External background sources . . . . .	14
1.6.3	Beta-neutron cascades . . . . .	15
1.6.4	External neutrons and correlated events . . . . .	16
1.7	Errors . . . . .	18
1.7.1	Detector systematic uncertainties . . . . .	18
1.7.2	Volume measurement . . . . .	18
1.7.3	Density . . . . .	19
1.7.4	Fraction of hydrogen atoms . . . . .	19
1.7.5	Gadolinium concentration . . . . .	19
1.7.6	Spatial effects . . . . .	19
1.7.7	Selection cuts uncertainties . . . . .	19
1.7.8	Background subtraction error . . . . .	22
1.7.9	Liquid scintillator stability and calibration . . . . .	23
1.8	Sensitivity and Expectations . . . . .	23
<b>2</b>	<b>U.S. Systems</b>	<b>27</b>
2.1	Inner Detector Photomultiplier Tubes . . . . .	27
2.1.1	Required Coverage . . . . .	27
2.1.2	Requirements on Radiopurity . . . . .	28
2.1.3	Base Electronics . . . . .	30
2.1.4	Potting and Cabling . . . . .	31
2.1.5	The PMT Selection Process . . . . .	32
2.1.6	PMT Testing . . . . .	32
2.1.7	PMT Mounting, Cleaning, and Assembly . . . . .	33
2.1.8	PMT Shipping, and Installation . . . . .	33
2.2	High Voltage System . . . . .	34
2.3	Outer Veto . . . . .	35
2.3.1	Expected Backgrounds . . . . .	35
2.3.2	Mechanical Constraints . . . . .	35
2.3.3	Detector Design . . . . .	36

2.3.4	Electronics . . . . .	36
2.4	Electronics . . . . .	39
2.4.1	HV-Splitters . . . . .	39
2.4.2	Front-End Electronics . . . . .	39
2.4.3	Trigger . . . . .	39
2.4.4	PMT rate monitor . . . . .	40
2.5	Slow Monitoring . . . . .	44
2.5.1	Monitoring via 1-Wire interface . . . . .	44
2.5.2	Radon monitoring . . . . .	46
2.5.3	Interface to other subsystems . . . . .	47
2.6	Laser System . . . . .	48
2.7	Calibration Deployment . . . . .	49
2.7.1	Introduction . . . . .	49
2.7.2	Deployment Methods . . . . .	49
2.7.3	Detector Interface . . . . .	50
2.7.4	Control Systems . . . . .	51
2.8	Radiopurity maintenance . . . . .	52
2.8.1	Potential for contamination from $^{222}\text{Rn}$ , $^{85}\text{Kr}$ , and dust . . . . .	52
2.8.2	Control measures . . . . .	53
<b>3</b>	<b>Cost and Schedule</b>	<b>54</b>
3.1	Overview of Costs . . . . .	54
3.2	Overview of Schedule . . . . .	54
3.3	Work Breakdown Structure (WBS) . . . . .	54
3.3.1	Work Breakdown Structure Description . . . . .	54
3.3.2	Full WBS . . . . .	57
3.4	Cost & Schedule Details . . . . .	58
3.4.1	Project Construction Schedule . . . . .	59
3.5	Project Management . . . . .	60
<b>A</b>	<b>The U.S. Collaboration</b>	<b>67</b>
<b>B</b>	<b>The Full Collaboration</b>	<b>67</b>

# Executive Summary

## Opportunity

There has been superb progress in understanding the neutrino sector of elementary particle physics in the past few years. It is now widely recognized that the possibility exists for a rich program of measuring CP violation and matter effects in future accelerator  $\nu$  experiments, using superbeams, off-axis detectors, neutrino factories and beta beams. However, this possibility can be fulfilled only if the value of the neutrino mixing parameter  $\theta_{13}$  is such that  $\sin^2(2\theta_{13}) \gtrsim 0.01$ . A new experiment at CHOOZ will be sensitive over most of that range,  $\sin^2(2\theta_{13}) > 0.03$  and has a great opportunity for an exciting and important discovery, a non-zero value to  $\theta_{13}$ . It would also serve as a crucial stop toward a more sensitive new experiment. In comparison to other possible sites, the far detector lab at CHOOZ already exists. It is possible, for a modest total cost, and a U.S. contribution of around \$5M, to rapidly deploy Double-CHOOZ and start taking data by 2008. The sensitivity of the original CHOOZ experiment would be surpassed in only 4 months. The full sensitivity of Double-CHOOZ would be reached in 3 years. Double-CHOOZ presents an ideal opportunity to leverage the US experience in neutrino detection with the European resources of nuclear reactor and neutrino laboratory as well as their expertise in low background detectors.

## Purpose of the Experiment

In the presently accepted paradigm to describe the neutrino sector, there are three mixing angles. One is measured by solar neutrinos and the KamLAND experiment, one by atmospheric neutrinos and the long-baseline accelerator projects. Both angles are large. The third angle,  $\theta_{13}$ , has not yet been measured to be nonzero but has been constrained to be small by CHOOZ.

## From CHOOZ to Double-CHOOZ

The basic feature of reactor  $\theta_{13}$  experiments is to search for energy dependent  $\bar{\nu}_e$  disappearance. CHOOZ used a single five-ton detector when the reactors were new. We propose to use two significantly-improved detectors (hence the name “Double-CHOOZ”) with increased luminosity. The best current limit on  $\theta_{13}$  comes from the CHOOZ experiment and is a function of  $\Delta m_{atm}^2$ , which has been measured using atmospheric neutrinos by Super-Kamiokande. The latest reported value of  $\Delta m_{atm}^2$  is  $1.2 < \Delta m_{atm}^2 < 3.0 \times 10^{-3} \text{eV}^2$  with a best fit reported at 2.0. The CHOOZ limits for  $\Delta m_{atm}^2$  of 2.6 and  $2.0 \times 10^{-3} \text{eV}^2$  are  $\sin^2(2\theta_{13}) < 0.14$  and 0.19. Global fits using the solar data limit the value for small  $\Delta m_{atm}^2$  to less than 0.12. The dominant systematic errors, such as cross-sections, flux uncertainties, and the absolute target volume, will be eliminated in a relative measurement with two identical detectors. Increased statistics will be achieved by running longer and using a larger detector, and with both CHOOZ reactors running at full power. In three years, Double-CHOOZ will achieve 250 t GW y (ton-Gigawatt-years) while the CHOOZ value was 12 t GW y. This will permit a mixing angle sensitivity of  $\sin^2(2\theta_{13}) > 0.03$ .

## Organization of the Proposal

The design of the Double-CHOOZ experiment is described in Section 1. Many parts of the Section draw on the previous European LOI, which was written with substantial input by some members of the US collaboration. Proposed US systems are described in Section 2. These are the inner detector photomultiplier tubes, the high voltage system, electronics, slow monitoring, a laser system, calibration deployment and radiopurity maintenance. In Section 3, we present the costs and schedule for the experiment, with emphasis on the U.S. components which are presented in this proposal. The management structure for the U.S. collaboration within Double-CHOOZ is included.

# 1 Description of the Double-CHOOZ Experiment

## 1.1 Introduction

A group of European scientists is proposing a new two-detector experiment known as Double-CHOOZ[4] at the Chooz-B Nuclear Power Station, the site of a previous reactor neutrino oscillation experiment, in order to search for a non-zero value of the mixing angle  $\theta_{13}$ . The collaboration, which currently consists of 52 physicists from 14 institutions in Europe, has received preliminary approval in France, a critical first step. Information about the physics opportunity, detector design and simulation, liquid scintillator and buffer liquids, calibration, backgrounds, systematic errors, and sensitivity are provided in the document “Letter of Intent for Double-CHOOZ: A Search for the Mixing Angle  $\theta_{13}$ ”[4]. The authors of this proposal are from U.S. institutions which have joined and are seeking funding. We review the motivation for such an experiment and its sensitivity in Section 1. The systems that the U.S. groups are proposing to work on are described in Section 2. The cost and schedule are provided in Section 3. A list of collaborators and a brief background of U.S. participants are given in an Appendix.

The members of this proposal have participated in the International Working Group with the goal of carrying through an experimental reactor neutrino program sensitive to  $\sin^2 2\theta_{13} > 0.01$ . Reaching such a sensitivity at the level of better than 1% is a difficult task as it requires total systematic uncertainties at the 1% level, something which has never been achieved in a reactor experiment. Double-CHOOZ, with an expected sensitivity of  $\sin^2 2\theta_{13} > 0.03$ , is an important step in this program for two reasons: (1) by exploring the region  $0.03 < \sin^2 2\theta_{13} < 0.2$  there is an excellent chance for a new discovery, and (2) it is a realistic setting to learn more about backgrounds and systematic errors crucial for mounting a more sensitive next-generation experiment. Concerning the last point, a number of initiatives are being considered that could potentially improve the Double-CHOOZ sensitivity by running longer with larger detectors located at greater depths[5, 6, 7, 8, 9]. These more sensitive experiments have greater cost, longer time scale, and are a more challenging extrapolation from previous experiments. In contrast, Double-CHOOZ can be done at modest cost and on a relatively short time scale using an existing facility. Double-CHOOZ will provide a crucial bridge to more ambitious and more sensitive experiments in the future.

## 1.2 Physics Motivation

In the presently accepted paradigm to describe the neutrino sector, there are three mixing angles ( $\theta_{12}$ ,  $\theta_{23}$ ,  $\theta_{13}$ ) that quantify the mixing of the neutrino mass and flavor eigenstates.  $\theta_{12}$  has been measured by solar neutrino experiments and the KamLAND reactor experiment.  $\theta_{23}$  has been measured by atmospheric neutrino experiments and the K2K long-baseline experiment. The third angle,  $\theta_{13}$ , has not yet been measured but has been constrained to be small by the CHOOZ reactor experiment[10].

The possibility exists for a rich program of measuring CP violation and matter effects in future accelerator neutrino experiments, which has led to an intense worldwide effort to develop neutrino superbeams, off-axis detectors, neutrino factories, and beta beams[11]. However, the possibility of measuring CP violation in the foreseeable future can be fulfilled only if the value of the neutrino mixing parameter  $\theta_{13}$  is such that  $\sin^2 2\theta_{13} \gtrsim 0.01$ . A timely new reactor experiment sensitive to  $\theta_{13}$  in this range has excellent discovery potential for finding a non-zero value of this important parameter. In addition, a short time scale for a measurement or improved limit on  $\theta_{13}$  will help

long-baseline accelerator experiments better exploit their full potential.

### 1.2.1 $\bar{\nu}_e$ detection principle

Reactor antineutrinos are detected through their interaction by inverse neutron decay (threshold of 1.806 MeV)

$$\bar{\nu}_e + p \rightarrow e^+ + n . \quad (1)$$

If we use an averaged fuel composition typical during a reactor cycle corresponding to  $^{235}\text{U}$  (55.6%),  $^{239}\text{Pu}$  (32.6%),  $^{238}\text{U}$  (7.1%) and  $^{241}\text{Pu}$  (4.7%), the mean energy release per fission  $W$  is 203.87 MeV and the energy weighted cross section amounts to  $\langle \sigma \rangle_{\text{fission}} = 5.825 \times 10^{-43} \text{ cm}^2$  per fission . For the purpose of simple scaling, a reactor with a power of 1  $\text{GW}_{th}$  induces a rate of  $\sim 450$  events per year in a detector containing  $10^{29}$  protons, at a distance of 1 km.

Experimentally one takes advantage of the coincidence signal of the prompt positron followed in space and time by the delayed neutron capture. This very clear signature allows us to reject most of the accidental backgrounds. The energy of the incident antineutrino is then related to the energy of the positron by the relation

$$E_{\bar{\nu}_e} = E_{e^+} + (m_n - m_p) + O(E_{\bar{\nu}_e}/m_n) . \quad (2)$$

Experimentally, the visible energy seen in the detector is given by  $E_{vis} = E_{e^+} + 511 \text{ keV}$ , where  $E_{e^+}$  is the sum of the rest mass and kinetic energy of the positron. and the additional 511 keV come from the annihilation of the positron with an electron when it stops in the matter.

### 1.2.2 $\bar{\nu}_e$ oscillations

Reactor neutrino disappearance experiments measure the survival probability  $P_{\bar{\nu}_e \rightarrow \bar{\nu}_e}$  of the electron antineutrinos emitted from the nuclear power plant. A disappearance experiment does not measure the  $\delta$ -CP phase. Furthermore, because of the low energy as well as the short baseline considered, matter effects are negligible[12]. Assuming a ‘‘normal’’ mass hierarchy scenario the  $\bar{\nu}_e$  survival probability can be written[13, 14]

$$\begin{aligned} P_{\bar{\nu}_e \rightarrow \bar{\nu}_e} &= 1 - 2 \sin^2 \theta_{13} \cos^2 \theta_{13} \sin^2 \left( \frac{\Delta m_{31}^2 L}{4E} \right) \\ &- \frac{1}{2} \cos^4 \theta_{13} \sin^2(2\theta_{12}) \sin^2 \left( \frac{\Delta m_{21}^2 L}{4E} \right) \\ &+ 2 \sin^2 \theta_{13} \cos^2 \theta_{13} \sin^2 \theta_{12} \left( \cos \left( \frac{\Delta m_{31}^2 L}{2E} - \frac{\Delta m_{21}^2 L}{2E} \right) - \cos \left( \frac{\Delta m_{31}^2 L}{2E} \right) \right) \end{aligned} \quad (3)$$

The first two terms in Equation 3 contain respectively the atmospheric driven ( $\Delta m_{31}^2 = \Delta m_{atm}^2$ ) and solar driven ( $\Delta m_{21}^2 = \Delta m_{sol}^2$ ,  $\theta_{12} \sim \theta_{sol}$ ) contributions, while the third term is an interference between solar and atmospheric driven oscillations whose amplitude is a function of  $\theta_{13}$ . Reactor experiments provide a clean measurement of the mixing angle  $\theta_{13}$ , free from any contamination coming from matter effects and other parameter correlations or degeneracies[12, 15].

## 1.3 Configuration of the Detectors for Double-CHOOZ

### 1.3.1 The CHOOZ nuclear reactors

The antineutrinos are produced by the pair of reactors located at the CHOOZ-B nuclear power station operated by the French company Electricité de France (EDF) in partnership with the Belgian utilities Electrabel S.A./N.V. and Société Publique d'Electricité. They are located in the Ardennes region, northeast of France, very close to the Belgian border, in a loop of the Meuse river (See Figure 1. Both reactors are of the most recent N4 type (4 steam generators) with a thermal power of  $4.27 \text{ GW}_{th}$ , and  $1.5 \text{ GW}_e$ . They operate with an 80% load factor. These are Pressurized Water Reactors (PWR) and are fed with UOx fuel. 205 fuel assemblies are contained within each reactor core. The entire reactor vessel is a cylinder of 13.65 meters high and 4.65 meters in diameter. The first reactor started operating at full power in May 1997, and the second one in September 1997.

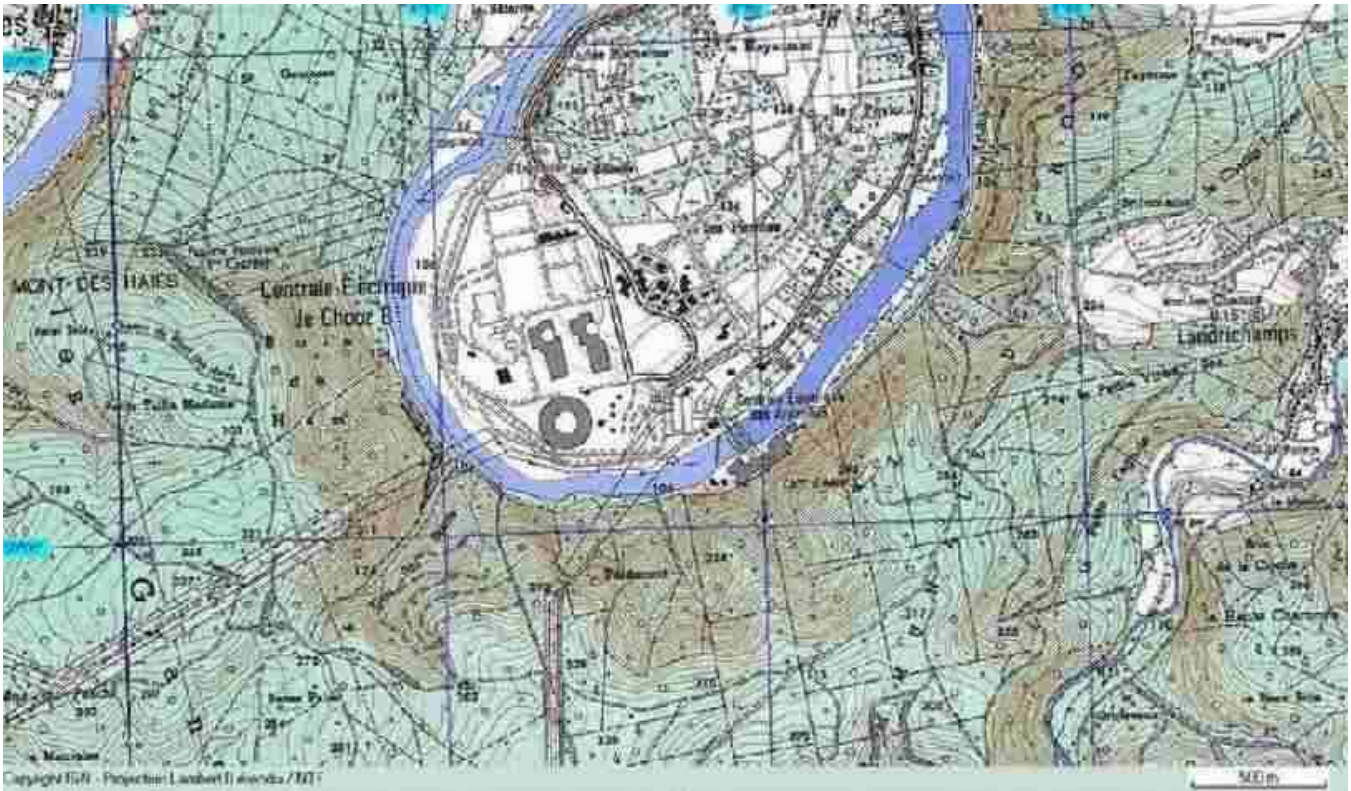


Figure 1: Map of the experiment site. The two cores are separated by a distance of 100 meters. The far detector site is located at 1.0 and 1.1 km from the two cores.

The Double-CHOOZ experiment will run two identical detectors of medium size, containing 12.7 cubic meters of liquid scintillator target doped with 0.1% of Gadolinium. The neutrino laboratory of the CHOOZ experiment, located 1.0 and 1.1 km respectively from the two cores of the CHOOZ nuclear plant will be used again (see Figure 2).

A sketch of the Double-CHOOZ far detector is shown in Figure 3. The CHOOZ far site is shielded by about 300 m.w.e. of  $2.8 \text{ g/cm}^3$  rocks. An artificial overburden of a few tens of meters height has to be built for the CHOOZ-near detector. The required overburden ranges from 53 to 80 m.w.e. depending on the near detector location, between 100 and 200 meters away from the cores. A



Figure 2: Picture of the CHOOZ far detector site taken in September 2003. The original CHOOZ laboratory hall constructed by EDF, located close the the old CHOOZ-A underground power plant, is still in perfect condition and will be re-used.



sketch of this detector is shown in Figure 4. An initial study has been commissioned by the French electricity power company EDF to determine the best combination of location-overburden and to optimize the cost of the project.

### 1.3.2 Detector design

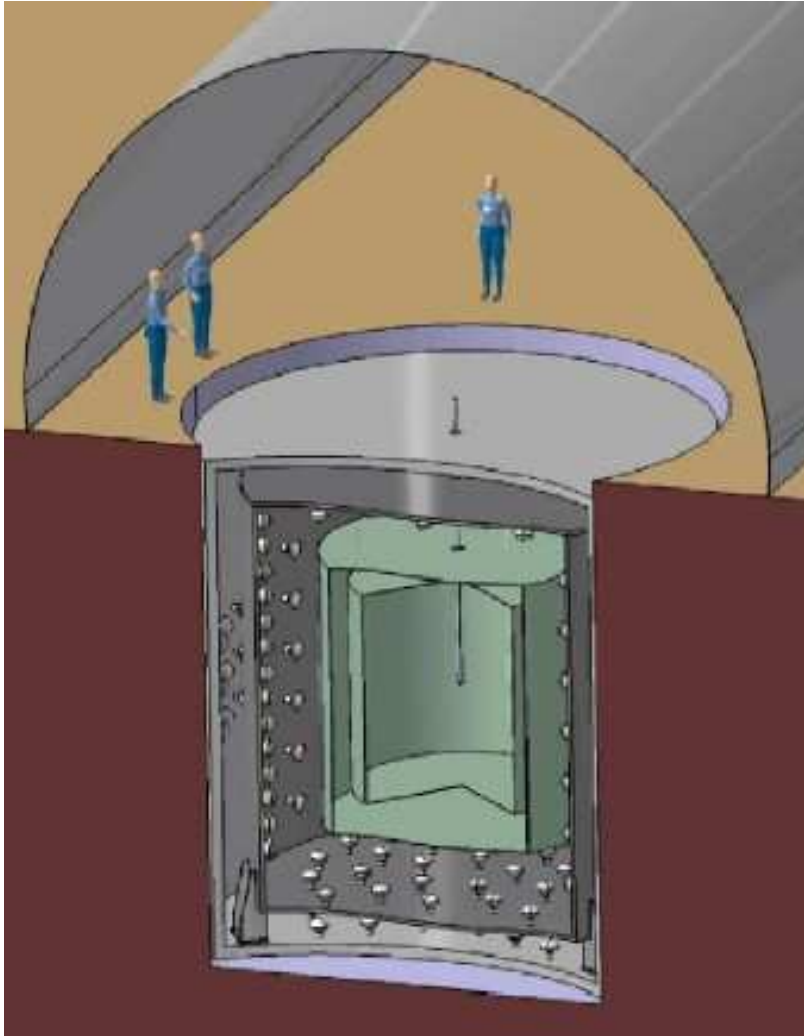


Figure 3: The Double-CHOOZ far detector, at the CHOOZ underground site. The detector is located in the tank used for the CHOOZ experiment (7 meters high and 7 meters in diameter) that is still available. About  $12.7 \text{ m}^3$  of a dodecane+PXE based liquid scintillator doped with gadolinium will be contained in a transparent acrylic cylinder surrounded by the  $\gamma$ -catcher region and the buffer.

The Double-CHOOZ far detector will consist of a target cylinder of 120 cm radius and 280 cm height, providing a volume of  $12.7 \text{ m}^3$ . The near and far detectors will be identical inside the PMTs supporting structure. This will allow a relative normalization systematic error of  $\sim 0.6\%$ . However, due to the different overburdens (60-80 to 300 m.w.e.), the outer shielding will not be identical since the cosmic ray background varies between Double-CHOOZ near and Double-CHOOZ far. The

overburden of the near detector has been chosen in order to keep the signal to background ratio above 100. In this case, a knowledge of the backgrounds within a factor two keeps the associated systematic error well below one percent.

Starting from the center of the target the detector elements are as follows (see Figures 3, 4 and 5).

- **$\bar{\nu}_e$  target** (12.7 m<sup>3</sup>)  
A 120 cm radius, 280 cm height, 6-10 mm width acrylic cylinder, filled with 0.1% Gd loaded liquid scintillator target (see Section 1.4).
- **$\gamma$ -catcher** (28.1 m<sup>3</sup>)  
A 60 cm buffer of non-loaded liquid scintillator with the same optical properties as the  $\bar{\nu}_e$  target (light yield, attenuation length). This scintillating buffer around the target is necessary to measure the gammas from the neutron capture on Gd, to measure the positron annihilation, and to reject the background from fast neutrons.
- **Non Scintillating Buffer** (100 m<sup>3</sup>)  
A 95 cm thick cylindrical buffer of non scintillating liquid, to decrease the level of accidental background (mainly the contribution from photomultiplier tubes radioactivity).
- **PMT supporting structure**
- **Inner Veto system**(100 m<sup>3</sup>)  
A 60 cm thick cylindrical veto region filled with liquid scintillator for the far detector, and a slightly larger one (about 100 cm) for the near detector.
- **Outer Veto system**(5000 tubes)  
A four-layer proportional tube system will identify and locate throughgoing muons with 98% efficiency.

Table 1 summarizes the control of the systematic uncertainties that was achieved in the CHOOZ experiment as well as the goal for Double-CHOOZ. The main uncertainties at CHOOZ came from the uncertainty in the knowledge of the antineutrino flux coming from the reactor. This systematic error vanishes by adding a near detector. The non-scintillating buffer will reduce the singles rates in each detector by two orders of magnitude with respect to CHOOZ, which had no such buffer. The positron detection threshold will be about 500 keV, well below the 1.022 MeV physical threshold of the inverse beta decay reaction. Such a low threshold has three advantages:

- The systematic error due to this threshold is suppressed. It was an 0.8% source of systematic error in CHOOZ[16].
- Backgrounds below 1 MeV reactor neutrino threshold can be measured.
- The onset of the positron spectrum provides an additional calibration point between the near and far detectors.

This reduction of the singles events relaxes or even suppresses the localization cuts that were used in CHOOZ[16] such as the distance of an event to the PMT surface and the distance between the positron and the neutron. These cuts were difficult to calibrate. Factors affecting other cuts will be

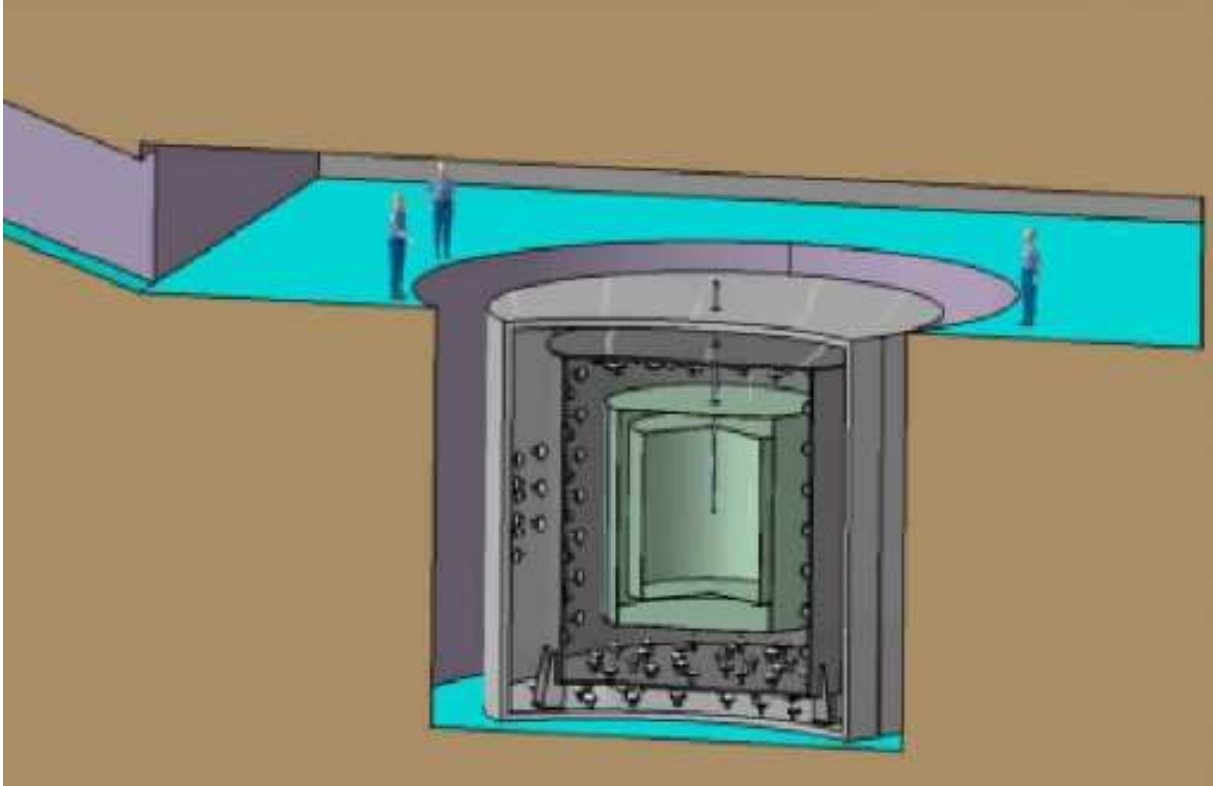


Figure 4: The CHOOZ-near detector at the new underground site, close to the reactor cores. This detector is identical to the Double-CHOOZ far detector up to and including the PMT surface. The veto region will be enlarged to better reject the cosmic muon induced backgrounds (see Section 1.6).

carefully calibrated between the two detectors. Most important will be the calibration of the energy selection of the delayed neutron after its capture on a Gd nucleus (with a mean energy release of 8 MeV in gammas). The requirement is  $\sim 100$  keV on the precision of this cut between both detectors, which is feasible with standard techniques using radioactive sources (energy calibration) and lasers (optical calibrations) at different positions throughout the detector active volume. The sensitivity of a reactor experiment of Double-CHOOZ scale ( $\sim 300$  GW<sub>th</sub>·ton·year) is mostly given by the total number of events detected in the far detector. The requirement on the positron energy scale is then less stringent since the weight of the spectrum distortion is low in the analysis.

A summary of key detector parameters is given in Table 2.

	CHOOZ	Double-CHOOZ
Reactor fuel cross sections	1.9%	—
Number of protons	0.8%	0.2%
Detection efficiency	1.5%	0.5%
Reactor power	0.7%	—
Energy per fission	0.6%	—

Table 1: Summary of the systematic errors in CHOOZ and the goals for Double-CHOOZ.

$\bar{\nu}_e$ far detector events	60,000	
$\bar{\nu}_e$ near detector events	3 Million	
Far Detector Distance	1.05 km	
Far Detector Overburden	300 m.w.e.	
$\bar{\nu}_e$ target volume	12.67 m <sup>3</sup>	Gd loaded LS (0.1%)
$\bar{\nu}_e$ target dimensions	120 cm × 280 cm	radius × height
$\gamma$ catcher volume	28.1 m <sup>3</sup>	unloaded LS
$\gamma$ catcher thickness	60 cm	
Buffer volume	100 m <sup>3</sup>	non-scintillating organic liquid
Veto volume	110 m <sup>3</sup>	low scintillating organic liquid
Near Detector Distance	100-200 m	
Near Detector Overburden	50-80 mwe	
Signal to Noise Goal	100:1	
Thermal Power	4.25 Gw	each of 2 cores
Electric Power	1.3 GWe	each of 2 cores
Running time at full power	3 years	
Number of Phototubes	512 8"	per detector
Phototubes Coverage	12.9%	
$\sin^2(2\theta)$ goal in 3 years	0.03	(90% CL)

Table 2: Summary of the some parameters of the proposed Double-CHOOZ experiment.

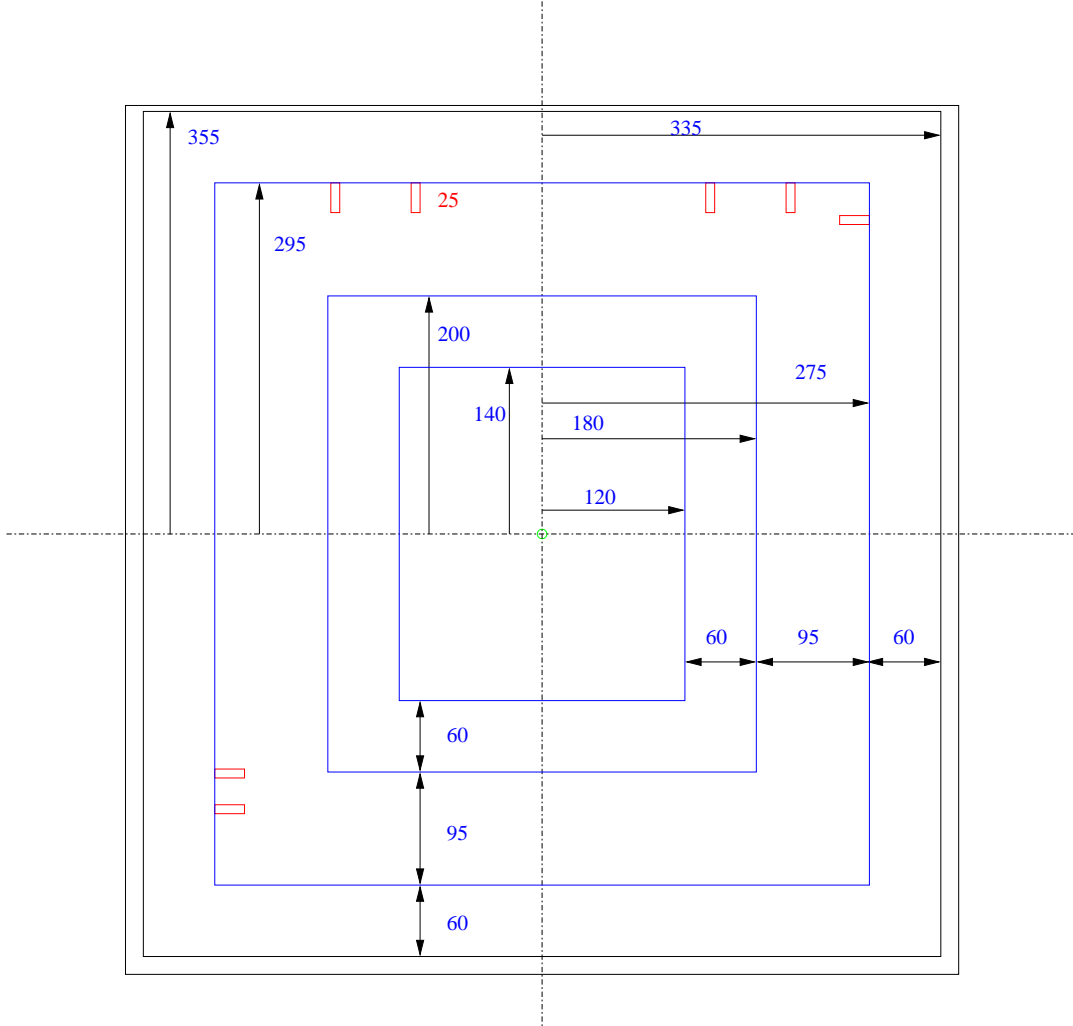


Figure 5: Dimensions of the Double-CHOOZ far detector (in cm). Starting from the center we have: the neutrino target region composed of Gd doped liquid scintillator ( $12.7 \text{ m}^3$ ), the  $\gamma$ -catcher region composed of unloaded liquid scintillator ( $28.1 \text{ m}^3$ ), the non scintillating buffer region ( $100.0 \text{ m}^3$ ), and the veto ( $110.0 \text{ m}^3$ ). The CHOOZ-near detector is identical up to and including the PMT support structure; however, its external muon veto is slightly larger to better reject the cosmic muon induced backgrounds.

## 1.4 Scintillator

### 1.4.1 Liquid inventory

The Double-CHOOZ detector design requires different liquids in the separate detector volumes as shown in Figures 3 and 4. The inner most volume of 12.7 m<sup>3</sup>, the  $\bar{\nu}_e$ -target, contains a proton rich liquid scintillator mixture loaded with gadolinium (Gd-LS) at a concentration of approximately 1 g/liter. The neutron capture time in 0.1% Gd loaded scintillator is 30 $\mu$ s. The adjacent volume, the  $\gamma$ -catcher, has a volume of 28 m<sup>3</sup> and is filled with an unloaded liquid scintillator. The photomultipliers are immersed in a non-scintillating buffer in order to shield the active volume from the gamma rays emitted by them. The volume of the buffer liquid is approximately 100 m<sup>3</sup>. Last, an instrumented optically isolated volume of approximately 110 m<sup>3</sup> encloses the whole setup serving as a shield against external radiation and as a muon veto system. Table 2 includes a summary of the liquid inventory of a single detector system.

The selection of the organic liquids are guided by physical and technical requirements, as well as by safety considerations. In particular, the solvent mixtures or their components have a high flash point (e.g. phenyl-xylylethane (PXE): flash point (fp) 145 °C, dodecane: fp 74 °C, mineral oil: fp 110 °C). The  $\bar{\nu}_e$ -target and  $\gamma$ -catcher have as solvent a mixture of 80% dodecane and 20% PXE, or alternatively trimethyl-benzene (PC). Mineral oil is under study as an alternative to dodecane. A similar solvent mixture matching the density of the  $\gamma$ -catcher and  $\bar{\nu}_e$ -target, will be used as the buffer liquid, however with the addition of a scintillation light quencher (e.g. DMP). The veto volume contains low-scintillating organic liquid and will be equipped with PMTs.

Research with gadolinium loaded scintillator at MPIK and LNGS/INR indicates that suitable gadolinium loaded scintillators can be produced using the chemistry of beta-diketone complexes as well as using a single carboxylic acid stabilized by careful control of pH. Several prototype detectors filled with different scintillator samples are continuously measured in the LENS low-background facility at Gran Sasso since October 2003 to study the stability of the scintillator as well as backgrounds. No change in light yield nor in attenuation length has been observed. Furthermore, research is being carried out to achieve stability with respect to interaction with detector container materials, through the adjustment of inert solvent components of the scintillator while simultaneously retaining high scintillation yields. A variety of tests have been carried out to date that show satisfactory optical properties using either Beta-diketonate (BDK) Gd-LS or Carboxylate (CBX) Gd-LS [4].

From the results of the laboratory research, we now have two working Gd-LS formulations and we expect that both the BDK and CBX systems will comply with the design goals of Double-CHOOZ. The designation of the default and backup LS formulation will take place in 2005. A further outcome is the detailed engineering of the Gd-LS production scheme. This will be a critical input for the finalization of the scintillator fluid systems discussed in the next subsection. The final selection of the buffer and veto liquids will be done contingent upon the mechanical design of the containment vessels and the definition of the Gd-LS formulation.

### 1.4.2 Scintillator fluid systems

The scintillator fluid systems (SFSs) include the **off-site SFS** for production, purification and storage of the Gd-LS, as well as the  $\gamma$ -catcher LS. The **on-site SFS** will be on the reactor area, close to the experimental location.

The SFSs scheme envisions the production and storage of the complete Gd-LS for both the near

and far detector, in order to assure identical *proton per volume* concentrations. The off-site SFS will include ISO-containers for storage and subsequent transport to the experimental site. Moreover, it will include a purification column, a nitrogen purging unit, a mixing chamber, nitrogen blankets and auxiliary systems. A similar system, known as Module-0[17], has been constructed by groups associated with Borexino. Since the specifications for Module-0 are more demanding than required for Double-CHOOZ, no problems are anticipated.

The on-site SFSs will consist of an area above ground close to the detector sites for the transport tanks which will be connected to the detector by a tubing system. The purpose of the on-site SFS is to transfer the different liquids from their transport container into the detector volumes in a safe and clean way. The different detector volumes will be filled simultaneously and kept at equal hydrostatic pressures.

## 1.5 Calibration

The main goal of the calibration effort is to reach maximum sensitivity to neutrino oscillations by comparing the positron energy spectra measured by the Double-CHOOZ far and Double-CHOOZ near detectors. Calculations show that a relative difference both in geometry (construction) and in response of detectors slightly distorts the ratio of the spectra in both detectors. Therefore, appropriate calibration coefficients and concise measurements of the systematic uncertainties need to be measured in situ. The calibration sources (See Table 3) must be deployed regularly throughout the detector active volume to monitor the detector response to positrons, neutron captures, gammas and the backgrounds in the Double-CHOOZ experiment. This requires a dedicated mechanical system in order to introduce calibration sources into the different regions of the detector.

There are a number of specific tasks for a successful calibration of the detectors. These include optical calibrations (single photoelectron (PE) response, multiple PE response, detector component optical constants), electronic calibrations (trigger threshold, timing and charge slopes and pedestals, dead time), energy (energy scale and resolution), and neutron and positron detection efficiency and response. In addition, detector calibrations test the Monte-Carlo and analysis code to verify the accuracy of the simulations, throughout the detector (spatially), and during the lifetime of the experiment.

The optical calibrations are based on the experience with CHOOZ and the CTF-Borexino experiments. In CTF-Borexino the optical calibration consists of a UV pulsed-laser (jitter less than 1 ns) coupled to an optical fiber illuminating separately each PMT. This allows the single PE response to be measured since the amplitude of the pulse is tuned to approximately a single PE. This technique allows the gain, timing slope, charge slope and pedestals to be determined relative to individual PMTs and to the triggers. In addition to the optical fiber calibration, the light attenuation in the liquid scintillator will be monitored using a diffusive laser ball source, as has been successfully used by many experiments over the last twenty years[18]. This source illuminates all the PMTs isotropically and allows the attenuation length of the detector components and the PMT angular response to be measured as a function of photon wavelength.

We will calibrate the detector energy response to gammas from 1 MeV to about 10 MeV corresponding to the endpoint of the fission product beta decays. It is necessary to also know the energy scale in the window 6-10 MeV to be able to identify the delayed second trigger as a neutron. The required accuracy is 100 keV. This will be accomplished by deploying various higher energy gamma calibration sources (see Table 3) and by detailed Monte-Carlo simulations in the energy region where there are no calibration sources.

Technique	Calibrations
Optical Fibers, Diffusive Laser ball	Timing and Charge Slopes and Pedestals, attenuation length of detector components
Neutron Sources: Am-Be, $^{252}\text{Cf}$	Neutron response, relative and absolute efficiency, capture time
Positron Sources: $^{22}\text{Na}$ , $^{68}\text{Ge}$	$e^+$ response, energy scale, trigger thresh.
Gamma Sources:	Energy linearity, stability, resolution, spatial and temporal variations.
$^{137}\text{Cs}$	$\beta^-$ , 0.662 MeV
$^{22}\text{Na}$	$\beta^+$ , 1.275 MeV + annih
$^{54}\text{Mn}$	EC, 0.835 MeV
$^{65}\text{Zn}$	1.35 MeV
$^{60}\text{Co}$	EC, 1.173, 1.33 MeV
$^{68}\text{Ge}$	EC, $\beta^+$ 1.899 MeV + annih
$^{88}\text{Y}$	EC, 0.898, 1.836 MeV
H neutron capture	2.223 MeV
$^{241}\text{Am}$ - $^9\text{Be}$	( $\alpha$ ,n) 4.44 MeV ( $^{12}\text{C}$ )
Gd neutron capture	Spectrum in 8 MeV window
$^{12}\text{C}$ neutron capture	4.97 MeV
$^{228}\text{Th}$	2.615 MeV
$^{40}\text{K}$	EC, $\beta^+$ , $\beta^-$ , 11% 1.46 MeV

Table 3: Table showing the different techniques that are available to calibrate the Double-CHOOZ experiment.



The overall energy scale can be determined from the position of the 0.662 MeV peak of the  $^{137}\text{Cs}$  source, and then verified by calibration with several gamma sources (see Table 3) in different energy ranges:  $^{54}\text{Mn}$  (0.835 MeV),  $^{65}\text{Zn}$  (1.351 MeV),  $^{60}\text{Co}$ , and  $^{228}\text{Th}$  (2.614 MeV). The capture of neutrons from an Am-Be source scintillator (to be discussed later) can also be used as a high energy gamma source as it produces prompt 4.4 MeV gammas. We will also use the natural sources from radioactive impurities of the detector materials ( $^{40}\text{K}$ ,  $^{208}\text{Tl}$ ) and neutrons produced by cosmic muons for energy calibration. Since these sources are present permanently, they are useful for monitoring the stability of the energy response.

Positron detection can be calibrated with a  $^{22}\text{Na}$  source. It emits a 1.275 MeV primary gamma accompanied by a low energy positron which annihilates inside the source container. The primary and annihilation gammas from the source mimic the positron annihilation resulting from an antineutrino event inside the detector. Another positron source is  $^{68}\text{Ge}$ , which produces positrons with higher energies, and therefore calibrates higher energy positrons.  $^{68}\text{Ge}$  decays by EC to  $^{68}\text{Ga}$  and  $\beta^+$ -decays to stable  $^{68}\text{Zn}$  with an endpoint of 1.9 MeV. This isotope also has the advantage that it produces only low energy gammas in coincidence with the nuclear decay, and the  $\beta^+$  has an endpoint of 1.889 MeV 89% of the time. A second purpose of this source (if a source is constructed so that the beta is absorbed by the shielding surrounding the source) is to tune the trigger threshold to be sensitive to annihilation gammas and to monitor its stability. A  $^{68}\text{Ge}$  source was successfully used in the Palo Verde reactor neutrino experiment [19].

There are two suitable and accessible neutron sources for neutron calibration: the Am-Be source and  $^{252}\text{Cf}$  spontaneous fission source. These sources emit neutrons with different energy spectra from what is expected from inverse beta decay, and thus the importance of these differences needs to be quantified. To decrease the background during neutron source deployment, neutrons from Am-Be should be tagged by the 4.4 MeV gamma emitted in coincidence with the neutron. This will allow the neutron capture detection efficiency to be determined independent of knowing the precise rate of the neutron source, because every time a 4.44 MeV gamma is detected a neutron is released [20]. It should be noted that the use of this gamma involves a significant correction for the n-p elastic scattering which often takes place in coincidence, thus the uncertainty is typically larger than for single gamma sources. The absolute neutron detection efficiency will be determined with a  $^{252}\text{Cf}$  source by using the known neutron multiplicity (known to 0.3%). For the source placed in the center, the size of the Gd region will be larger than the neutron capture mean free path, so that the neutron capture will be studied independent of the presence of the acrylic vessel. In order to tag the neutron events, a small fission chamber will be used to detect the fission products. Therefore, neutron source calibrations will provide us with the relevant data to calibrate the detector response to neutrons. In particular, neutron sources will allow us to measure the absolute neutron efficiency, to determine and monitor the appropriate thresholds of neutron detection, and to measure the neutron capture time for both the far and near detectors.

## 1.6 Background

The signature for a neutrino event is a prompt signal with a minimum energy of about 1 MeV and a delayed 8 MeV signal after neutron capture in gadolinium. This may be mimicked by background events which can be divided into two classes: accidental and correlated events. The former occur when a neutron like event by chance falls into the time window (typically few 100  $\mu\text{s}$ ) after an event in the scintillator with an energy of more than one MeV. The latter is formed by neutrons which slow down by scattering in the scintillator, deposit  $> 1$  MeV visible energy and are captured

in the Gd region. The sources and rates of various backgrounds are used in this subsection to determine the necessary overburden of the near detector and the purity limits for detector components.

### 1.6.1 Intrinsic backgrounds

Background due to beta and gamma events above about 1 MeV can take place in the scintillator or in the acrylic vessels which contain the liquid. The contribution from the Uranium and Thorium chains is reduced to a few elements, as all alpha events show quenching with visible energies well below 1 MeV. Furthermore the short delayed Bi-Po coincidences in both chains can be detected event by event, and hence rejected. The decays of  $^{234}\text{Pa}$  (beta decay,  $Q = 2.2$  MeV),  $^{228}\text{Ac}$  (beta decay,  $Q = 2.13$  MeV) and  $^{208}\text{Tl}$  (beta decay,  $Q = 4.99$  MeV) need to be considered. Assuming radioactive equilibrium the beta/gamma background rate due to both chains can be estimated by  $b_1 \simeq M_U \cdot 6 \cdot 10^3 \text{ s}^{-1} + M_{Th} \cdot 4 \cdot 10^3 \text{ s}^{-1}$ , where the total mass of U and Th is given in grams. Taking into account the total scintillator mass of the neutrino target plus the  $\gamma$ -catcher, this rate can be expressed by  $b_1 \simeq 3 \text{ s}^{-1}(c_{U,Th}/10^{-11})$ , where  $c_{U,Th}$  is the mass concentration of Uranium and Thorium in the liquid.

The contribution from  $^{40}\text{K}$  can be expressed by  $b_2 \simeq 1 \text{ s}^{-1}(c_K/10^{-9})$ , where  $c_K$  is the mass concentration of natural K in the liquid. The background contribution due to U, Th and K in the acrylic vessels can be written as  $b_3 \simeq 2 \text{ s}^{-1}(a_K/10^{-7}) + 5 \text{ s}^{-1}(a_{U,Th}/10^{-9})$ , where  $a_K$  and  $a_{U,Th}$  describe the mass concentrations of K, U and Th in the acrylic. Measured values of  $a$  in the CTF of Borexino and by SNO show that in principle the beta/gamma rate in the detector due to intrinsic radioactive elements can be kept at levels well below  $1 \text{ s}^{-1}$ .

The dominant contribution to the external gamma background is expected to come from the photomultipliers (PMTs) and structure material. Again contributions from U, Th and K have to be considered. However, because of the shielding of the buffer region only the 2.6 MeV gamma emission from  $^{208}\text{Tl}$  has to be taken into account. The shielding factor  $S$  due to the buffer liquid is calculated to be  $S \sim 10^{-2}$ . The resulting gamma background in the neutrino target plus the  $\gamma$ -catcher can be written as  $b_{ext} \simeq 2 \text{ s}^{-1}(N_{PMT}/500)$ , where  $N_{PMT}$  is the number of PMTs. Section 2.1 contains a more detailed study of this background.

Neutrons inside the target may be produced by spontaneous fission of heavy elements and by  $(\alpha,n)$ -reactions. For the rate of both contributions the concentrations of U and Th in the liquid are the relevant parameters. The neutron rate in the target region can be written as  $n_{int} \simeq 0.4 \text{ s}^{-1}(c_{U,Th}/10^{-6})$ . For the aimed concentration values the intrinsic contribution to the neutron background is negligible.

### 1.6.2 External background sources

Several sources contribute to the external neutron background. We first discuss external cosmic muons which produce neutrons in the target region via spallation and muon capture. Those muons intersect the detector and should be identified by the veto systems. However, some neutrons may be captured after the veto time window. Therefore we estimate the rate of neutrons, which are generated by spallation processes of through going muons and by stopped negative muons which are captured by nuclei.

The first contribution is estimated by calculating the muon flux for different shielding values and

taking into account an  $E^{0.75}$  dependence for the cross section of neutron production, where  $E$  is the depth dependent mean energy of the total muon flux. The absolute neutron flux is finally obtained by considering measured values in several experiments (LVD[21], MACRO[22], CTF[23]) in the Gran Sasso underground laboratory and extrapolating these results by comparing muon fluxes and mean energies for the different shielding factors. Table 4 gives the expected neutron rate depending on the shielding.

Overburden (m.w.e.)	$\mu$ rate ( $s^{-1}$ )	$\langle E_\mu \rangle$ (GeV)	Neutrons through going $\mu$ ( $s^{-1}$ )	$\mu$ stopping rate ( $s^{-1}$ )	Neutrons stopping $\mu$ ( $s^{-1}$ )
40	$1.1 \cdot 10^3$	14	2	$5 \cdot 10^{-1}$	0.7
60	$5.7 \cdot 10^2$	19	1.4	$3 \cdot 10^{-1}$	0.4
80	$3.5 \cdot 10^2$	23	1	$1.2 \cdot 10^{-1}$	0.2
100	$2.4 \cdot 10^2$	26	0.7	$6 \cdot 10^{-2}$	0.08
300	$2.4 \cdot 10^1$	63	0.15	$2.5 \cdot 10^{-3}$	0.003

Table 4: Estimated neutron rate in the active detector region due to through going cosmic muons.

Negative muons which are stopped in the target region can be captured by nuclei where a neutron is released afterward. The rate can be estimated quite accurately by calculating the rate of stopped muons as a function of the depth of shielding and taking into account the ratio between the  $\mu$ -life time and  $\mu$ -capture times. As the capture time in Carbon is known to be around  $25 \mu s$  ( $\approx 1$  ms in H) only about 10% of captured muons may create a neutron. Since the concentration in Gd is so low, its effect can be neglected here. The estimated results are shown in Table 4. The neutron generation due to through going muons dominates.

### 1.6.3 Beta-neutron cascades

Muon spallation on  $^{12}\text{C}$  nuclei in the organic liquid scintillator may generate  $^8\text{He}$ ,  $^9\text{Li}$ , and  $^{11}\text{Li}$  which may undergo beta decay with a neutron emission. Those background events show the same signature as a neutrino event. For small overburdens the muon flux is too high to allow tagging by the muon veto, as the lifetimes of these isotopes are between 0.1 s and 1 s. The cross sections for the production of  $^8\text{He}$ ,  $^9\text{Li}$  have been measured by a group of TUM at the SPS at CERN with muon energies of 190 GeV (NA54 experiment[24]). In this experiment only the combined production  $^8\text{He} + ^9\text{Li}$  were obtained without the ability to separate them.

A conservative estimate of 2 events per day in the target region can be estimated for 300 m.w.e. shielding by assuming  $E^{0.75}$  scaling as we did in calculating the neutron flux. An alternative scaling has been suggested whereby the number of  $^9\text{Li}/^8\text{He}$ -producing interactions varies in proportion to the flux of muons over 500 GeV[25], leading to a lower event rate of 0.4 per day.

In Table 5 all radioactive  $^{12}\text{C}$ -spallation products including the beta-neutron cascades are shown with the estimated event rates in both detectors.

The Q-values of the beta-neutron cascade decays is 8.6 MeV, 11.9 MeV, 20.1 MeV for  $^8\text{He}$ ,  $^9\text{Li}$ , and  $^{11}\text{Li}$ , respectively. In the experiment the  $^8\text{He}$  production rate might be measured if we set a dedicated trigger after a muon event in the target region looking for the double cascade of energetic betas ( $^8\text{He} \rightarrow ^8\text{Li} \rightarrow ^8\text{Be}$ ) occurring in 50% of all  $^8\text{He}$  decays. Nothing similar exists in the case of

${}^9\text{Li}$ , but the beta endpoint here is above the positron endpoint induced by reactor antineutrinos. KamLAND has measured that the production of  ${}^9\text{Li}$  (lifetime 838 ms) dominates the production of  ${}^8\text{He}$  (lifetime 119 ms) by at least a factor of 8. Nevertheless, from the results of the NA54 experiment[24], the total cross section of  ${}^8\text{He} + {}^9\text{Li}$  is known, and if the  ${}^8\text{He}$  is evaluated separately, some redundancy on the total  $\beta$ -neutron cascade will be available. The neutrons emitted in the  ${}^8\text{He}$  decays are typically around 1 MeV. With an overburden more than 50 mwe, these backgrounds are acceptable.

Isotopes	Near detector		Far detector	
	$R_\mu$ ( $E^{0.75}$ scaling)	$R_\mu$ ( $E > 500$ GeV)	$R_\mu$ ( $E^{0.75}$ scaling)	$R_\mu$ ( $E > 500$ GeV)
${}^{12}\text{B}$		not measured		
${}^{11}\text{Be}$	< 18	< 3.8	< 2.0	< 0.45
${}^{11}\text{Li}$		not measured		
${}^9\text{Li}$	$17 \pm 3$	3.6	$1.7 \pm 0.3$	0.36
${}^8\text{Li}$	$31 \pm 12$	6.6	$3.3 \pm 1.2$	0.7
${}^8\text{He}$		${}^8\text{He} \ \& \ {}^9\text{Li}$ measured together		
${}^6\text{He}$	$126 \pm 12$	26.8	$13.2 \pm 1.3$	2.8
${}^{11}\text{C}$	$7100 \pm 455$	1510	$749 \pm 48$	159.3
${}^{10}\text{C}$	$904 \pm 114$	192	$95 \pm 12$	20.2
${}^9\text{C}$	$38 \pm 12$	8.1	$4.0 \pm 1.2$	0.85
${}^8\text{B}$	$60 \pm 11$	12.7	$5.9 \pm 1.2$	1.25
${}^7\text{Be}$	$1800 \pm 180$	382.9	$190 \pm 19$	40.4

Table 5: Radioactive isotopes produced by muons and their secondary shower particles in liquid scintillator targets at the Double-CHOOZ near and far detectors. The rates  $R_\mu$  (events/d) are given for a target of  $4.4 \times 10^{29}$   ${}^{12}\text{C}$  (For a mixture of 80% Dodecane and 20% PXE,  $12.7 \text{ m}^3$ ) at a depth of 60 m.w.e. for the near detector and 300 m.w.e. for the far detector. Columns 3 and 5 correspond to an estimate of the number of events assuming that the isotopes are produced only by high energy muon showers  $E > 500$  GeV[25]. A neutrino signal rate of 85 events per day is expected at Double-CHOOZ far, without oscillation effect (for a power plant running at nominal power, both dead time and detector efficiency are not taken into account here).

#### 1.6.4 External neutrons and correlated events

Very fast neutrons, generated by cosmic muons outside the detector, may penetrate into the target region. As the neutrons are slowed down through scattering, recoil protons may give rise to a visible signal in the detector. This is followed by a delayed neutron capture event. Therefore, this type of background signal gives the right time correlation and can mimic a neutrino event. Pulse shape discrimination in order to distinguish between  $\beta$  events and recoil protons is in principle possible, but will only be used as a consistency check since the errors are not small.

A Monte-Carlo program has been written to estimate the correlated background rate for a shielding depth of 100 m.w.e. and a flat topology. In order to test the code the correlated background

for the Chooz experiment (different detector dimensions, 300 m.w.e. shielding) has been calculated with the program. The most probable background rate was determined to be 0.8 counts per day. A background rate higher than 1.6 events per day is excluded by 90% C.L. This has to be compared with the measured rate of 1.1 events per day. We conclude that the Monte-Carlo program reproduces the real correlated background value roughly within a factor 2.

For Double-Chooz we calculated the correlated background rate for 100 m.w.e. shielding and estimated the rates for other shielding values by taking into account the different muon fluxes and assuming a  $E^{0.75}$  scaling law for the probability to produce neutrons. The neutron capture rate in the Gd loaded scintillator for an overburden of 100 m.w.e. is about 300/h. However, only 0.5% of those neutrons create a signal in the scintillator within the neutrino window (i.e. between 1 MeV and 8 MeV), because most deposit much more energy during the multiple scattering processes. The quenching factors for recoil protons and carbon nuclei has been taken into account. In addition around 75% from those events generate a signal in the inner muon veto above 4 MeV (visible  $\beta$  equivalent energy). In total the correlated background rate is estimated to be about 3 counts per day for 100 m.w.e. shielding. This can be measured to high precision using events tagged by the inner and/or outer veto. In Table 6 the estimated correlated background rates are shown for different shielding depths.

Overburden (m.w.e.)	Total neutron rate in $\nu$ -target ( $\text{h}^{-1}$ )	Correlated background rate ( $\text{d}^{-1}$ )
40	829	8.4
60	543	5.4
80	400	4.2
100	286	3.0
300	57	0.5

Table 6: Estimated neutron rate in the target region and the correlated background rate due to fast neutrons generated outside the detector by cosmic muons.

The correlated background rates can be compared with accidental rates, where a neutron signal falls into the time window opened by a  $\beta^+$ -like event. The background contribution due to accidental delayed coincidences can be determined *in situ* by measuring the single counting rates of neutron-like and  $\beta^+$ -like events. Therefore the accidentals are not so dangerous as correlated background events. Radioactive elements in the detector materials will be carefully controlled, especially in the scintillator itself, so the beta-gamma rate above 1 MeV will be only a few counts per second. For a time window for the delayed coincidence of  $\sim 200 \mu\text{s}$  (this should allow a highly efficient neutron detection in Gd loaded scintillators), and a veto efficiency of 98%, the accidental background rates are estimated in Table 7. The rate of neutrons which cannot be correlated to muons (“effective neutron rate”) is calculated by  $n_{eff} = n_{tot} \cdot (1 - \epsilon)$ , where  $n_{tot}$  is the total neutron rate (sum of the numbers given in Table 4) and  $\epsilon$  is the veto efficiency. If the veto efficiency is 98% or better, the accidental background for the far detector is far below one event per day (see following Table 7).

We conclude that correlated events are the most severe background source for the experiment. Two processes mainly contribute:  $\beta$ -neutron cascades and very fast external neutrons. Both types

Overburden (m.w.e.)	Effective neutron rate (h <sup>-1</sup> )	Accidental background rate (d <sup>-1</sup> )
40	97	2.4
60	65	1.6
80	43	1.0
100	28	0.7
300	6	0.15

Table 7: Example of estimated accidental event rates for different shielding depths. The rates scale with the total beta-gamma rate above 1 MeV (here  $b_{tot} = b_{ext} + b \approx 2.5 \text{ s}^{-1}$ ), the time window (here  $\tau = 200 \mu\text{s}$ ) and the effective neutron background rate. A muon veto efficiency of 98% was assumed.

of events are coming from spallation processes of high energy muons. In total the background rates for the near detector will be between 9/d and 23/d if a shielding of 60 m.w.e. is chosen. For the far detector a total background rate between 1/d and 2/d is estimated.

## 1.7 Errors

In the CHOOZ experiment, the total systematic error was 2.7%. The goal of Double-CHOOZ is to reduce the overall systematic uncertainty to 0.6%. A summary of the CHOOZ systematic errors is given in Table 1[16]. The right column presents the new experiment goals.

### 1.7.1 Detector systematic uncertainties

The distance from the CHOOZ detector to the cores of the nuclear plant was measured to within  $\pm 10$  cm. This translates into a systematic error of 0.15% in Double-CHOOZ, because the effect becomes relatively more important for the near detector located 100-200 meters away from the reactor. Specific studies are currently ongoing to guarantee this 10 cm error. Furthermore, the ‘‘barycenter’’ of the neutrino emission in the reactor core must be monitored with the same precision. In a previous experiment at Bugey[26], a 5 cm change of this barycenter was measured and monitored, using the instrumentation of the nuclear power plant[27]. Our goal is to confirm that this error could be kept below 0.2%.

### 1.7.2 Volume measurement

In the CHOOZ experiment, the volume measurement was done with an absolute precision of 0.3%[16]. The goal is to reduce this uncertainty by a factor of two, but only on the relative volume measurement between the two inner acrylic vessels (the other volumes do not constitute the  $\bar{\nu}_e$  target). We plan to use the same mobile tank to fill both targets; a pH-based measurement is being studied as well. A more accurate measurement could be performed by combining a traditional flux measurement with a weight measurement of the quantity of liquid entering the acrylic vessel. Furthermore we plan to build both inner acrylic targets at the manufacturer and to move each of them as a single unit to the detector site. Both inner vessels will undergo precise filling tests at the manufacturer.

### 1.7.3 Density

The uncertainty of the density of the scintillator is  $\sim 0.1\%$ . The target liquid will be prepared in a large single batch, so that they can be used for the two detector fillings. The same systematic effect will then occur in both detectors and will not contribute to the overall systematic error. However, the measurement and control of the temperature will be important to guarantee the stability of the density in both targets (otherwise it would contribute to the relative uncertainty, see Section 1.8). The temperature control and circulation of the liquid in the external veto will be used to keep both  $\bar{\nu}_e$  targets at a constant temperature.

### 1.7.4 Fraction of hydrogen atoms

This quantity is very difficult to measure, and the error is of the order of  $1\%$ ; however, the target liquid will be prepared in a large single batch (see above). This will guarantee that, even if the absolute value is not known to a high precision, both detectors will have the same number of hydrogen atoms per gram. This uncertainty, which originates in the presence of unknown chemical compounds in the liquid, does not change with time. The thermal neutron is captured either on hydrogen or on Gadolinium (other reactions such as Carbon captures can be neglected).

### 1.7.5 Gadolinium concentration

Gd concentration can be extracted from a time capture measurement done with a neutron source calibration. A very high precision can be reached on the neutron detection efficiency ( $0.3\%$ ) by measuring the detected neutron multiplicity from a Californium source (Cf). This number is based on the precision quoted in Reference [16], but taking away the Monte-Carlo uncertainty, since we work with two-identical detectors. We can increase our sensitivity to very small differences in the response from both detectors by using the same calibration source for the measurements. The Californium source calibration can be made all along the z-axis of the detector, and is thus sensitive to spatial effects due to the variation of Gd concentration (staying far enough from the boundary of the target, and searching for a top/down asymmetry). A difference between the time capture of both detectors could also be detected with a sensitivity slightly less than  $0.3\%$ .

### 1.7.6 Spatial effects

A major advantage of the three volume design for Double-CHOOZ is the absence of a fiducial volume cut. The entire inner volume is the fiducial volume, so the relative normalization depends on detector size and liquid measurement, and does not depend on phototube properties and detailed simulations.

The  $\sim 1\%$  spill in/out effect observed in the CHOOZ experiment[16] cancels by using a set of two identical detectors. An angle effect persists but is much smaller. A 500 keV energy cut induces a positron inefficiency smaller than  $0.1\%$ . The relative uncertainties between both detectors lead thus to an even smaller systematic error.

### 1.7.7 Selection cuts uncertainties

The analysis cuts are potentially important sources of systematic errors. In the CHOOZ experiment it was  $1.5\%$ [16]. The goal of the new experiment is to reduce this error by a factor of three. The

CHOOZ experiment used 7 analysis cuts to select the  $\bar{\nu}_e$  (one of them had 3 cases, see Section 8.7 of [16]). In Double-CHOOZ we plan to reduce the number of selection cuts to 3 (one of them will be very loose, and may not even be used). This can be achieved because of reduction of the number of accidentals background events, only possible with the new detector design. To select  $\bar{\nu}_e$  events we have to identify the prompt positron followed by the delayed neutron (delayed in time and separated in space). The trigger will require two local energy depositions of more than 500 keV in less than 200  $\mu$ s.

Since any  $\bar{\nu}_e$  interaction deposits at least 1 MeV (slightly less due to the energy resolution effect) the energy cut at 500 keV does not reject any  $\bar{\nu}_e$  events. As a consequence, there will not be any systematic error associated with the trigger. The only requirement is the stability of the energy threshold, which is related to the energy calibration.

The energy spectrum of a neutron capture has two peaks, the first peak at 2.2 MeV tagging the neutron capture on hydrogen, and the second peak at around 8 MeV tagging the neutron capture on Gd. The selection cut that identifies the neutron will be set at about 6 MeV, which is above the energy of neutron capture on hydrogen and all radioactive contamination. At this energy of 6 MeV, an error of  $\sim 100$  keV on the selection cut changes the number of neutrons by  $\sim 0.2\%$ . This error on the relative calibration is achievable by using the same Cf calibration source for both detectors.

The exact analytical behavior describing the neutron capture time on Gd is not known, so the absolute systematic error for a single detector cannot be significantly improved with respect to CHOOZ [16]. However, the uncertainty originating from the liquid properties disappears by comparing the near and far detector neutron time capture. The remaining effect deals with the control of the electronic time cuts. For completeness, a redundant system will be designed in order to control perfectly these selection cuts (for example time tagging in a specialized unit and using Flash-ADC's).

The distance cut systematic error (distance between prompt and delayed events) was published as 0.3% in the CHOOZ experiment [16]. This cut is difficult to calibrate, since the rejected events are typically  $\bar{\nu}_e$  candidates badly reconstructed. In Double-CHOOZ, this cut will be either largely relaxed (two meters instead of one meter for instance) or totally suppressed, if the accidentals event rate is low enough, as expected from current simulations).

The Double-CHOOZ veto will consist of liquid scintillator and have a thickness of 60 cm at the far site, and even larger at the near detector site. The veto inefficiency comes from the through going cables and the supporting structure material. This inefficiency was low enough in CHOOZ, and should be acceptable for the Double-CHOOZ far detector. However, it must be lowered for the near detector because the muon flux is a factor 30 higher for a shallower overburden of 60 m.w.e.. A constant dead time will be applied in coincidence with each through going muon. This has to be measured very carefully since the resulting dead time will be very different for the two detectors: a few percent at the far detector, and at around 30% at the near detector. A 1% precision on the knowledge of this dead time is required. This will be accomplished with several independent methods:

- the use of a synchronous clock, to which the veto will be applied,
- a measurement of the veto gate with a dedicated flash ADC,
- the use of an asynchronous clock that randomly generates two signals mimicking the antineutrino tag (with the time between them characteristic of the neutron capture on Gd). With



this method, all dead times (originating from the veto as well as from the data acquisition system) will be measured simultaneously. A few thousand such events per day are needed,

- the generation of sequences of veto-like test pulses (to compare the one predicted dead time to the actually measured).

The trigger will be rather simple. It will use only the total analog sum of energy deposit in the detector. Two signals of more than 500 keV in 200  $\mu$ s will be required.

A summary of the systematic errors associated with  $\bar{\nu}_e$  event selection cuts is given in Table 8. We summarize in Table 9 the systematic uncertainties that largely cancel in the Double-CHOOZ

	CHOOZ		Double-CHOOZ
selection cut	rel. error (%)	rel. error (%)	Comment
positron energy*	0.8	0	not used
positron-geode distance	0.1	0	not used
neutron capture	1.0	0.2	Cf calibration
capture energy containment	0.4	0.2	Energy calibration
neutron-geode distance	0.1	0	not used
neutron delay	0.4	0.1	—
positron-neutron distance	0.3	0 – 0.2	0 if not used
neutron multiplicity*	0.5	0	not used
combined*	1.5	0.2-0.3	—

\*average values

Table 8: Summary of the neutrino selection cut uncertainties. CHOOZ values have been taken from[16].

experiment. The error on the absolute knowledge of the chemical composition of the Gd scintillator

	CHOOZ	Double-CHOOZ
Reactor power	0.7%	negligible
Energy per fission	0.6%	negligible
$\bar{\nu}_e$ /fission	0.2%	negligible
Neutrino cross section	0.1%	negligible
Number of protons/cm <sup>3</sup>	0.8%	0.2%
Neutron time capture	0.4%	negligible
Neutron efficiency	0.85%	0.2%
Neutron energy cut ( $E_\gamma$ from Gd)	0.4%	0.2%

Table 9: Summary of systematic errors that cancel or are significantly decreased in Double-CHOOZ.

disappears. There remains only the measurement error on the volume of target (relative between two detectors). The error on the absolute knowledge of the gamma spectrum from a Gd neutron capture disappears. However, there will be a calibration error on the difference between the 6 MeV energy cut in both detectors. Table 10 summarizes the identified systematic errors that are currently being considered for the Double-CHOOZ experiment.

	After CHOOZ	Double-CHOOZ Goal
Solid angle	0.2%	0.2%
Volume	0.2%	0.2%
Density	0.1%	0.1%
Ratio H/C	0.1%	0.1%
Neutron efficiency	0.2%	0.1%
Neutron energy	0.2%	0.2%
Spatial effects	neglect	neglect
Time cut	0.1%	0.1%
Dead time(veto)	0.25%	< 0.25%
Acquisition	0.1%	0.1%
Distance cut	0.3%	< 0.2%
Grand total	0.6%	< 0.6%

Table 10: The column “After CHOOZ” lists the systematic errors that can be achieved without improvement of the CHOOZ published systematic uncertainties Reference [16]. In Double-CHOOZ, we estimate the total systematic error on the normalization between the detectors to be less than 0.6%.

### 1.7.8 Background subtraction error

The design of the detector will allow a Signal/Background (S/B) ratio of about 100 to be achieved (compared to 25 at full reactor power in the first experiment[16]). The knowledge of the background at a level around 30-50% will reduce the background systematic uncertainties to an acceptable level. In the Double-CHOOZ experiment, two background components have been identified, uncorrelated and correlated. Among those backgrounds, one has:

- The accidental rate, that can be computed from the single event measurements, for each energy bin.
- The fast neutrons creating recoil protons, and then a neutron capture. This background was dominant in CHOOZ[16]. The associated energy spectrum is relatively flat up to a few tens of MeV.
- The cosmogenic muon induced events, such as  ${}^9\text{Li}$  and  ${}^8\text{He}$ , that have been studied and measured at the NA54 CERN experiment[24] in a muon beam as well as in the KamLAND experiment[28]. Their energy spectrum goes well above 8 MeV, and follows a well defined shape.

The backgrounds that will be measured are:

- Below 1 MeV (this was not possible in CHOOZ, due to the different detector design and the higher energy threshold)
- Above 8 MeV (where there remains only 0.1% of the neutrino signal).
- By extrapolating from the various thermal power of the plant (refueling will result in two months per year at half power).

From the measurement of the energy spectrum in accidental events, and from the extraction of the cosmogenic spectrum, the shape of the spectrum for fast neutron events can be obtained with a precision greater than what is required.

### 1.7.9 Liquid scintillator stability and calibration

From our simulations, the calibration of the relative energy scales at the 1% level is necessary. The specification of no more than 100 keV scale difference at 6 MeV is achieved if this 1% level is obtained. This level of calibration can be obtained with the program considered in subsection 1.5. We will move the same calibration radioactive sources from one detector to the other, and directly compare the position of the well defined calibration peaks.

## 1.8 Sensitivity and Expectations

An overview of various predictions compiled for Reference [1] is given in Table 11. For more extensive reviews, see for example [29, 30, 31, 32]. The conclusion from all these considerations about neutrino mass models is that a value of  $\theta_{13}$  close to the CHOOZ bound would be quite natural, while smaller values become harder and harder to understand as the limit on  $\theta_{13}$  is improved. These predictions are graphically depicted in Figure 6.

The CHOOZ experiment[10], which provides the most sensitive limit on  $\theta_{13}$  to date, did not push the limit lower for two related reasons: (1) It met its goal of showing that the atmospheric neutrino anomaly was not due to  $\nu_{\mu} \rightarrow \nu_e$  oscillations and (2) It was close to its systematic error limit due to uncertainties in the reactor neutrino flux, and so stopped running. Double-CHOOZ will *cover* roughly 85% of the available parameter space in that graph and cover a similar percentage of those predictions. We emphasize that a non-zero value for  $\theta_{13}$  is expected, unlike the situation in most searches for new physics!

The best present CHOOZ limit on  $\theta_{13}$  is a function of  $\Delta m_{atm}^2$ , which has been measured using atmospheric neutrinos by Super-Kamiokande (SK) and others. The latest reported value from SK[61] is  $1.5 < \Delta m_{atm}^2 < 3.0 \times 10^{-3} eV^2$  with a best fit reported at  $2.4 \times 10^{-3} eV^2$ . The current CHOOZ limits for  $\Delta m^2$  of 3.0, 2.0, and  $1.5 \times 10^{-3} eV^2$  are  $\sin^2 2\theta_{13} < 0.12, 0.20,$  and 0.40 respectively. Figure 7 shows the limits expected from Double-CHOOZ after 3 years of operation as a function of  $\Delta m_{atm}^2$ , assuming  $\theta_{13}$  is zero. This depends strongly on the *relative* normalization systematic error between the near and far detectors ( $\sigma_{rel}$ ) which we estimate will be 0.5%. Double-CHOOZ will significantly improve the existing limits even if a positive value of  $\theta_{13}$  is not found.

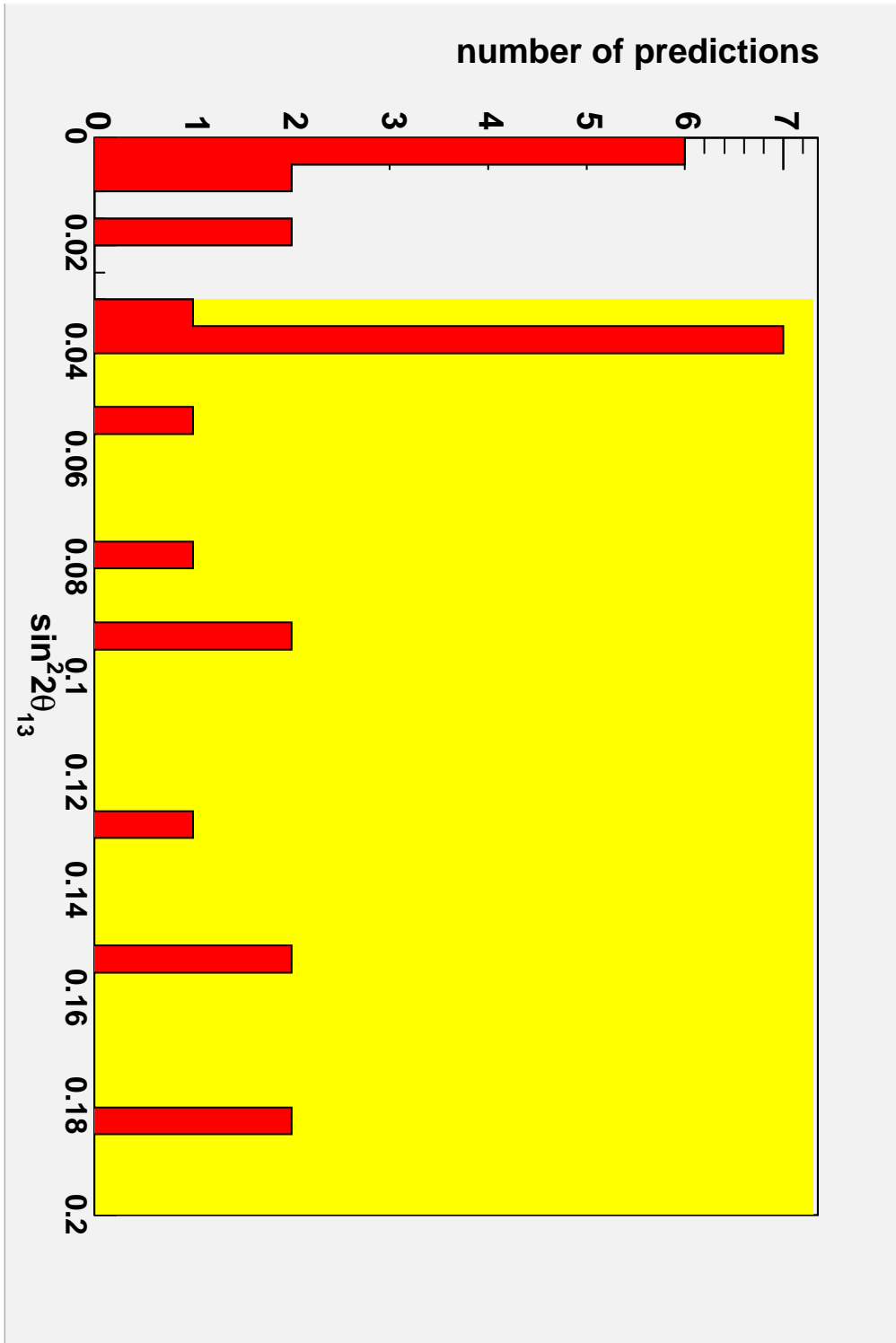


Figure 6: Predictions for  $\theta_{13}$ . The sensitive region of Double-CHOOZ is shown in yellow.

Reference	$\sin \theta_{13}$	$\sin^2 2\theta_{13}$
<i>SO(10)</i>		
Goh, Mohapatra, Ng [33]	0.18	0.13
<i>Orbifold SO(10)</i>		
Asaka, Buchmüller, Covi [34]	0.1	0.04
<i>SO(10) + flavor symmetry</i>		
Babu, Pati, Wilczek [35]	$5.5 \cdot 10^{-4}$	$1.2 \cdot 10^{-6}$
Blazek, Raby, Tobe [36]	0.05	0.01
Kitano, Mimura [37]	0.22	0.18
Albright, Barr [38]	0.014	$7.8 \cdot 10^{-4}$
Maekawa [39]	0.22	0.18
Ross, Velasco-Sevilla [40]	0.07	0.02
Chen, Mahanthappa [41]	0.15	0.09
Raby [42]	0.1	0.04
<i>SO(10) + texture</i>		
Buchmüller, Wyler [43]	0.1	0.04
Bando, Obara [44]	0.01 .. 0.06	$4 \cdot 10^{-4}$ .. 0.01
<i>Flavor symmetries</i>		
Grimus, Lavoura [45, 46]	0	0
Grimus, Lavoura [45]	0.3	0.3
Babu, Ma, Valle [47]	0.14	0.08
Kuchimanchi, Mohapatra [48]	0.08 .. 0.4	0.03 .. 0.5
Ohlsson, Seidl [49]	0.07 .. 0.14	0.02 .. 0.08
King, Ross [50]	0.2	0.15
<i>Textures</i>		
Honda, Kaneko, Tanimoto [51]	0.08 .. 0.20	0.03 .. 0.15
Lebed, Martin [52]	0.1	0.04
Bando, Kaneko, Obara, Tanimoto [53]	0.01 .. 0.05	$4 \cdot 10^{-4}$ .. 0.01
Ibarra, Ross [54]	0.2	0.15
<i>3 × 2 see-saw</i>		
Appelquist, Piai, Shrock [55, 56]	0.05	0.01
Frampton, Glashow, Yanagida [57]	0.1	0.04
Mei, Xing [58] (normal hierarchy)	0.07	0.02
(inverted hierarchy)	$> 0.006$	$> 1.6 \cdot 10^{-4}$
<i>Anarchy</i>		
de Gouvêa, Murayama [59]	$> 0.1$	$> 0.04$
<i>Renormalization group enhancement</i>		
Mohapatra, Parida, Rajasekaran [60]	0.08 .. 0.1	0.03 .. 0.04

Table 11: Incomplete selection of predictions for  $\theta_{13}$ .

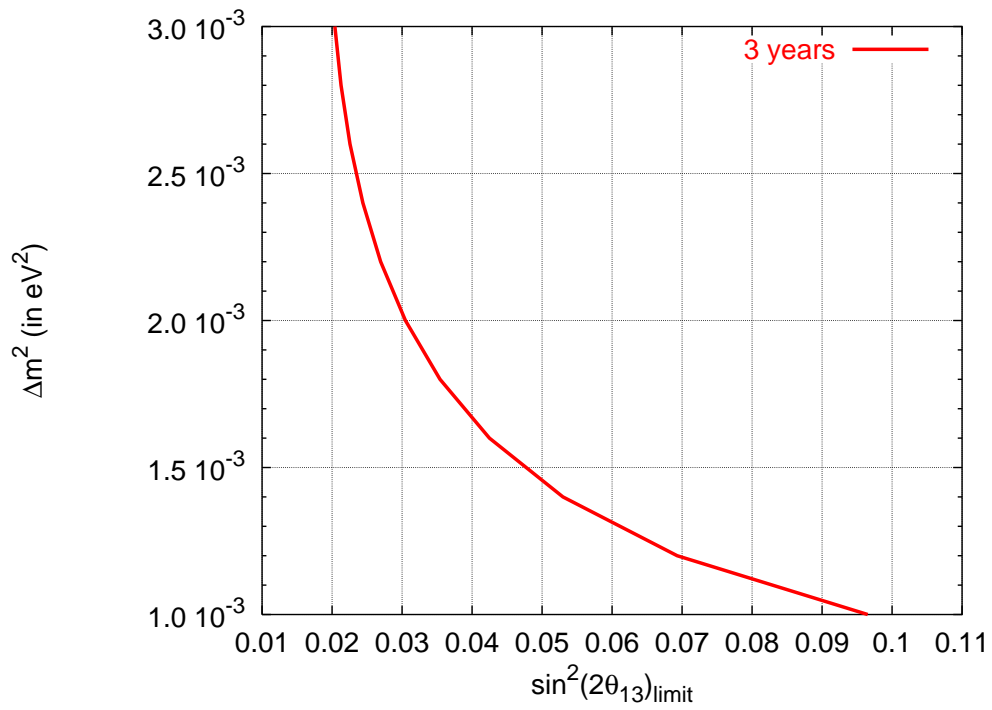


Figure 7: Double-CHOOZ sensitivity limit at 90% C.L. (for 1 d.o.f).

## 2 U.S. Systems

### 2.1 Inner Detector Photomultiplier Tubes

Photomultiplier tubes (PMTs) are a major component of the Double-CHOOZ detectors and will be a primary U.S. contribution to the experiment. We are proposing the purchase of 512 photomultiplier tubes each for the near and far Double-CHOOZ detectors, along with 16 spares for a total of 1040. There are several reasons why this area is highly appropriate as a U.S. responsibility:

- The U.S. Double-CHOOZ group has extensive experience in selection, testing, and mounting of PMTs, having participated in CHOOZ, E645, IMB, KamLAND, LSND, mini-BooNE, SNO, and Super-Kamiokande.
- It is a crucial part of the experiment that lends itself easily to being done in the U.S. and shipped pre-assembled to the Chooz site.
- At the end of the experiment, the PMTs can be recovered for re-use in other experiments. As an example, the IMB PMTs are still in use after almost twenty years! Thus purchase of these large, hemispherical, low-background PMTs can be viewed as a long-term investment in the U.S. program.

Double-CHOOZ will have two PMT regions: (1) Inner Detector (ID) PMTs to view the neutrino target and gamma-catcher region, and (2) Inner Veto (IV) PMTs to view an active outer veto layer. In this proposal, we present plans to construct the ID PMT array only. It is expected that construction of the IV array will be done by European collaborators. This is a natural separation, since the ID array must detect relatively low light levels and be compatible with the radiological standards of the target region, while the IV array will be operating in the high light levels from cosmic-ray muons and can have more relaxed radiological specifications. It is possible that different PMTs might be used for these two arrays.

There are many factors and trade-offs involved in the design of an ID PMT array for Double-CHOOZ. One important consideration is PMT size. For a given collection area, larger PMTs are favored over smaller ones due to their somewhat lower cost per area and the reduced number of electronics and high-voltage channels required. However, this must be balanced with the difficulty in the handling and mounting of large PMTs in a confined space, the increased background due to higher glass/area ratio, and the potential “hole” in coverage from the loss of a single PMT. Experiments requiring large-area coverage (e.g. Super-Kamiokande) have used the largest PMTs available (twenty inches) while experiments requiring less coverage (e.g. CHOOZ) have selected smaller PMTs (eight inches). In this proposal we consider the use of eight-inch PMTs similar to the original CHOOZ experiment, although the possibility for larger (thirteen-inch) PMTs is still being explored. The PMT budget of this proposal is conservative in the sense that selection of the larger PMTs would be less expensive.

#### 2.1.1 Required Coverage

The required PMT coverage is based on three factors: (1) adequate light collection to allow a hardware threshold well below 1 MeV, (2) sufficient energy resolution to reject backgrounds above

Table 12: Assay of the U, Th, K content of an ETI9354 PMT

material	component	mass	K (mg) (+/-)		Th ( $\mu$ g) (+/-)		U ( $\mu$ g) (+/-)	
bialkali	photocathode		2					
glass	envelope	635	38	10	19	6	19	13
	base (no pins)	10	1	0	0	0	0	0
ceramics	sideplates	10	0	0	1	0	0	0
	rods/spacers	13	0	0	1	0	0	0
metals	dynodes	86.6	0	1	3	1	0	1
	generator	0.4	10	1	0	0	0	0
plastics	overcap	32	5	2	1	0	1	0

the neutron capture gamma energy window at 8 MeV, and (3) adequate energy resolution to allow shape comparison between the visible energy spectrum in the near and far detectors. For Double-CHOOZ the first two reasons dominate, as our simulations show very little change in sensitivity over reasonable values of energy resolution at 1 MeV.

Simulations of the required coverage are notoriously difficult since they must fold together light production efficiency, transport through the waveshifter-laced scintillator (including re-emission of previously shifted light), optical effects of the acrylic vessels, transport through oil, and reflections from the walls and other structures. As an example of the difficulty, pre-experiment simulations for KamLAND predicted roughly 100-150 p.e./MeV (using only 17-inch PMTs), whereas about 240 p.e./MeV was realized in the actual experiment.

### 2.1.2 Requirements on Radiopurity

PMTs are typically one of the most radioactive materials used in the construction of neutrino detectors. This is due to the fact that they may contain 1 kg of glass per PMT - and glass typically has a rather high concentration of the long-lived elements uranium (U), Thorium (Th), and potassium (K). For example, Table 12 shows the radioactive assay of the Electron Tubes, Inc. (ETI) model 9354 developed for use in the Borexino experiment.

The most important backgrounds come from the decay of  $^{40}\text{K}$  and  $^{208}\text{Tl}$  (part of the thorium chain).  $^{40}\text{K}$  has a single 1.46 MeV gamma from electron capture to the first excited state of  $^{40}\text{K}$ .  $^{208}\text{Tl}$  has many possible gammas from beta decay to excited states of  $^{208}\text{Pb}$ , but all of them go through the first excited state at 2.61 MeV. Figure 8 shows the gamma energy spectrum from a GEANT3 simulation of the Double-CHOOZ detector backgrounds.

Based on these data, each PMT has a total  $^{40}\text{K}$  activity of 1.77 Hz. Taking into account a branching ratio of 0.1067 for EC capture to the first excited state gives a gamma activity of 0.19 Hz. Assuming secular equilibrium with  $^{232}\text{Th}$ , the  $^{208}\text{Tl}$  total activity is 0.097 Hz, with a gamma



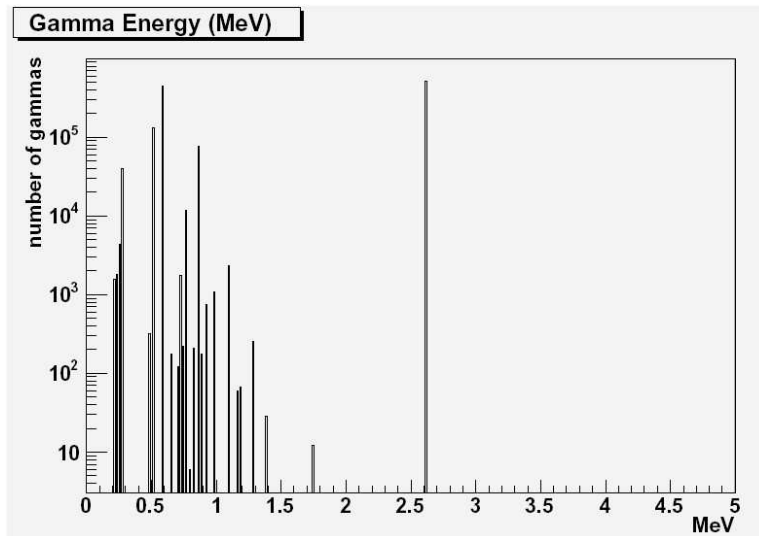


Figure 8: Simulation of the energy spectrum of  $^{208}\text{Th}$  gamma rays from beta decay to  $^{208}\text{Pb}$ .

activity of 0.23 Hz per PMT.

Using the detector simulation to propagate these gammas from the PMTs to the scintillator-filled volumes results in the energy spectrum of Figure 9. In this spectrum, the energy used is the summed energy of all the gammas as they enter the active volumes so that the effect of correlated gammas is included. In addition, the electrons from the beta decay are also included, as they may produce gammas from bremsstrahlung. Knowing the absolute activity then allows the number of events above a given energy threshold to be extracted from this figure. Above 0.5 MeV we therefore expect 2.7 Hz of gammas and above 1.0 MeV we expect 1.7 Hz.

To estimate the number of background events that come from this activity requires an estimate of the background from other sources in the 8 MeV range (the energy of neutron capture on gadolinium). There are two major sources: (1) neutrons produced from muon spallation or muon capture, and (2) external gammas in the range of 8 MeV produced by nearby untagged muons. The rate of (1) is given in Table 4 of Section 1 and is about 6 (65)  $h^{-1}$  for the far (near) detector. The rate of (2) can be estimated from the original CHOOZ experiment, about 180  $h^{-1}$  at 300 m.w.e. Conservatively scaling from the muon rate gives 4300  $h^{-1}$  in the near detector (assuming 60 m.w.e.). With a 200  $\mu\text{sec}$  window, the expected background rate from the accidental coincidence of a neutron-like event with a PMT-generated gamma is about 1.5 (18)  $d^{-1}$  for the far (near) detector. This is to be compared with an expected signal rate of about 65 (3500)  $d^{-1}$  (including efficiency). In practice, the accidental rate can be measured to high precision using non-coincidental singles rates and spectrum. If a 1% measurement is made, then using ETI9354 PMTs would contribute an uncertainty of only 0.02% to the experimental result. Since uncertainties below 0.05% have a negligible effect of the results, we adopt the assay requirements of Table 13 as specifications for total PMT activity. These are essentially the summed values of Table 12 multiplied by two.

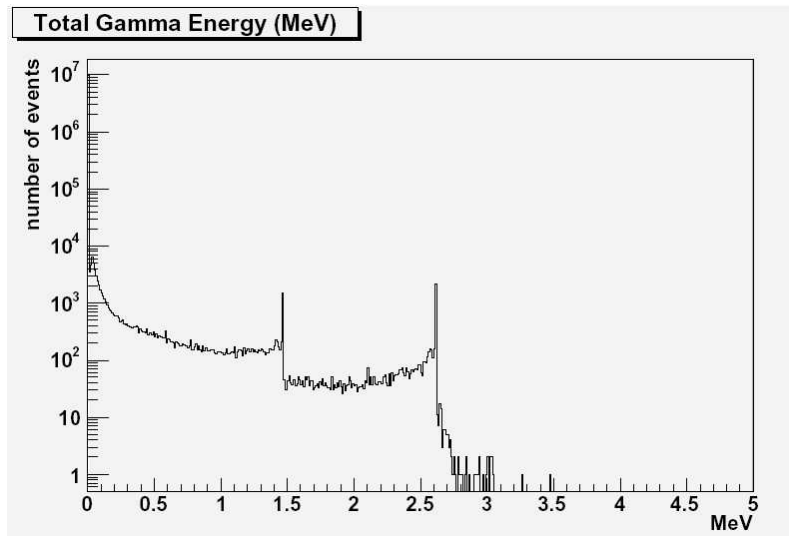


Figure 9: Simulation of the energy spectrum of gamma rays from  $^{40}\text{K}$  and  $^{208}\text{Tl}$  which enter the scintillator volumes.

Table 13: Specifications for the allowed U, Th, K content per PMT

chain	specification
uranium	$40 \mu\text{g}$
thorium	$50 \mu\text{g}$
potassium	$110 \text{mg}$

In addition to the ETI PMT, Hamamatsu Corporation also offers low-radioactivity 8-inch tubes. They have agreed to supply us with a sample of such a PMT and we intend to assay it using the low background counting facility at Alabama.

### 2.1.3 Base Electronics

We intend to use traditional passive divider chains similar to those used in the Super-Kamiokande outer detector (designed at Louisiana State University) and KamLAND. Since they consist only of resistors and capacitors, the reliability is very high. This is important since we plan to pot the electronics in epoxy (see below) so a failure would be impossible to repair.

We plan to operate the PMTs at a gain such that a single photoelectron pulse into 50 ohms produces roughly a 20 mV pulse. At this value, simple, commercially-available discriminators work well, pulse heights are large compared with typical noise levels and HV ripple and dark noise values

are typically negligible compared to rates from low-energy singles. The exact gain will depend on the model of PMT selected and the details of the front-end electronics design. Louisiana State University will work with Drexel in the specification and design of the divider chain electronics.

We also plan to back-terminate the divider chain in order to reduce the multiple reflections that can result from the large pulses generated when a muon passes through the scintillator. This requires operating at an increased gain to make up for signal loss, but the reduced dead time loss more than makes up for this. A typical muon pulse is expected to result in 200-300 p.e. per PMT, on average. This means a pulse height in the several volt range as compared to around 100 mV or so for typical neutrino interactions.

Currently, we plan to have the PMT supplier also build and attach the divider chains according to our specifications. This is to allow them to pot the electronics at the factory, which is very desirable from the standpoint of catching defective PMTs before delivery and ensuring quality control. This was done by both the Super-Kamiokande and KamLAND experiments and proved to be very satisfactory.

#### 2.1.4 Potting and Cabling

In order to reduce the amount of cabling in the Double-CHOOZ detector, we plan to have a single 50-ohm coaxial cable carrying both high voltage and signal from the PMT to a patch panel above the detector. This is essentially the scheme used in the Super-Kamiokande outer detector as well as LSND and MiniBooNE. The patch panel will not only allow picking off of the signal for routing to the front-end electronics, but also allow a transition from an expensive Teflon-coated jacket (made for long-term oil immersion) to a cheaper PVC jacket.

We plan to purchase PMTs with the divider electronics already potted for immersion in oil. The 17-inch PMTs for KamLAND and the 8-inch PMTs for the Super-Kamiokande veto were purchased in a similar fashion and the results were very satisfactory, with less than 1% failure after immersion. We have also determined from comparing quotes from one supplier with our experience in potting the KamLAND 20-inch PMTs ourselves that the costs are very similar.

The potting is done by first attaching a small circuit board containing the divider electronics to the pins of the PMT via floating leads instead of sockets. This prevents any residual stress from unseating the PMT. Then the electronics and PMT are aligned in an injection mold and a high-viscosity, oil-resistant epoxy is bonded to the PMT, cable, and circuit board in a single operation. For KamLAND, this was done by Hamamatsu using A Nippon Pelnox two-component epoxy MG-151/HY-306. This epoxy is not only oil-resistant but also has a high electrical resistance of more than  $10^{10}$  Ohm-cm and a low density of about 1.1 g/cm.

While this specific epoxy has worked well in the KamLAND oil, the Double-CHOOZ oil will be slightly different and thus we will test this material for compatibility before use. Louisiana State University has experience in this area.

### 2.1.5 The PMT Selection Process

We plan to select the PMT type for Double-CHOOZ on the basis of several criteria:

- proven compliance with our low activity specifications
- proven ability to attach and pot diver chain electronics to our specifications
- satisfactory peak-to-valley ratio (typically 2 or more) to allow us to balance PMT gains and aid in energy calibration
- proven quantum efficiency ( $> 20\%$ ) and reasonable transit time jitter (few ns) with full-face illumination
- price

Test setups for PMT performance at Louisiana State University and PMT radioactivity at Alabama will ensure PMTs meet basic specifications and will be used for quality control during the testing, cleaning, and assembly of the PMTs.

An important consideration is whether the supplier can deliver PMTs at a rate needed for the Double-CHOOZ construction schedule. Based on our experience, it typically takes about four months for a factory to tool up an assembly line, and normally they can make about 200 PMTs per month. Two potential suppliers that were contacted have confirmed this estimate. Thus, to meet the construction schedule that calls for far detector operation beginning in summer 2007, we must order the PMTs by November 2005.

### 2.1.6 PMT Testing

We plan to have the PMTs shipped first to Louisiana State University, where a high-throughput testing facility will be constructed similar to those used in IMB, Super-Kamiokande, and KamLAND. PMTs will be tested for gain and dark noise versus high voltage, and an initial operating voltage selected that will balance the PMT gains. Defective PMTs will also be identified and returned to the factory.

To meet the construction schedule, we must test 60 PMTs/week. Since each test requires a preceding dark period of roughly 24 hours, we need to make a facility capable of testing about twelve PMTs at a time (allowing the weekends to be used to make-up any failed tests).

After electronics testing, the PMTs will be driven in batches of 100 to Alabama for cleaning, mounting, and radioactivity spot-checking.

### 2.1.7 PMT Mounting, Cleaning, and Assembly

According to the present mechanical design, the ID PMTs will be mounted looking straight ahead on rails with the spacing between PMTs optimized from simulation studies. The rails will be provided as part of the PMT support structure built by the French collaborators. The design of the PMT mounts will be adapted from the designs successfully implemented by other experiments, e.g. MiniBooNE, using the same basic type of PMT in a similar environment. The mount materials and the fabrication process will be chosen to meet chemical compatibility requirements and radiological standards.

Prototype mounts will be built in the University of Alabama Physics machine shop and test assembled with PMTs. These assemblies will be placed in a dark box, powered, and counted over a long period (at least one month) to check that addition of the mounts does not damage the PMTs. In addition, a mount will be shipped to France for checking that it can be mounted to the rail system. Once the design and fabrication process is finalized, the job of making 1040 mounts from materials provided by the University of Alabama group will be handed over to an outside shop.

The PMTs received from Louisiana State University and the completed PMT mounts will be cleaned and assembled by the University of Alabama group. A clean area with forced ventilation through high efficiency filters will be set up in one of the labs. A team of undergraduate and graduate students will degrease the PMT mounts with acetone, pass them through an ultrasound bath in weak acid, rinse in water, and then thoroughly wipe down the mounts with alcohol. The PMTs will also be wiped down with alcohol. Within one hour of each being wiped down with alcohol, the PMT and its mount will be assembled, wiped down again with alcohol, allowed to dry, and then sealed in plastic. The wipe tissues from alcohol cleaning of the first assemblies will be counted in the University of Alabama low background Ge detector to check that no significant surface radio-contamination survives to final cleaning. Wipe tissues will be spot-checked throughout the cleaning and assembly stage. Manpower will be assigned to cleaning and assembly to keep pace with PMT shipments from Louisiana State University.

### 2.1.8 PMT Shipping, and Installation

The PMT–mount assemblies will be individually packed into boxes and shipped to Argonne, which will be the staging point for shipment of Double-CHOOZ detector components to France. Installation of the PMTs onto the support system rails will be the responsibility of the Louisiana State University and the University of Alabama groups.

## 2.2 High Voltage System

A single vendor will be chosen to provide all of the major high voltage components for the Double-CHOOZ PMT system. Two very similar HV systems will be installed, one each at the near and far detector sites. One mainframe and one module type will be used throughout the system. Common software will be written to meet the controls, monitoring and safety requirements as described elsewhere in this document. This will simplify the system in general, which should result in a lower initial cost as well as reduced maintenance costs. We will consider all reasonable vendors but the two primary candidates are Connecticut-based Universal Voltronics (UV) and CAEN from Italy. We have requested budgetary pricing information from these two vendors and the information we have received has been included in the WBS section 3.4. Since the exact number of channels is unknown at this time, we requested pricing for 1070 channels of high voltage, rated at <3000 VDC @ 2.5mA/ch. This section and its corresponding WBS elements include information for the inner detector PMTs only. The PMT vendor will attach and pot the special 20-meter HV/signal cables to the PMT assemblies.

## 2.3 Outer Veto

Due to the shallow depth at the near detector, a high rate of muons is expected. Since the primary background signal for this measurement will be initiated by cosmic muons, an additional outer veto system is required. This will be used to help identify muons which could cause neutrons or other cosmogenic backgrounds and allow them to be eliminated from the data set. In some sense, the outer veto provides redundancy for the inner veto in tagging background associated coincidences, but such a redundancy is crucial to making a confident measurement of the background. Comparison of a single measurement with a full simulation would not provide such confidence because the cross sections for muon spallation products are not accurately measured. In addition, the outer veto will provide two other benefits: 1) it will achieve a tracking resolution not possible with the inner veto alone, reducing the volume of the inner detector that is “deadened” by a muon passing through, and 2) it will well measure those muons which only clip the corners of the inner veto. Such muons are especially dangerous because the inner veto efficiency will be low for these. The goal is to provide a system with  $4\pi$  coverage and greater than 98% efficiency.

### 2.3.1 Expected Backgrounds

Many sources of backgrounds have been investigated in the Double-CHOOZ LOI [4]. The most significant were identified as coincident backgrounds arising from cosmic muons. The primary, and highest rate, are fast neutrons. These fast neutrons are spallation products from through-going muons in the surrounding rock. The neutrons can penetrate the detector and interact with a nucleus in the target region, providing a prompt signal, and then become captured by Gadolinium, providing the delayed signal.

A secondary background, which will also be difficult to identify, results from high energy muons which pass directly through the target region and interact with  $^{12}\text{C}$  nuclei in the target. This can produce radioactive isotopes of He and Li which undergo beta decay with a subsequent neutron emission. The beta-neutron signal will provide an identical signature to the positron-neutron signal from a neutrino event. Unfortunately, simply tagging the muon will not allow the elimination of these radioactive events since the half-lives of these isotopes are between 0.1 - 1 second. Thus any veto system will require some form of timing and pointing or tracking to be able to correlate a coincident signal with a previously through-going muon.

### 2.3.2 Mechanical Constraints

The near detector laboratory has not yet been constructed. Therefore the mechanical possibilities for a veto system are relatively open. Given the shallow depth, we expect a significant muon rate from a wide angular region of space. It has been estimated that using a full  $4\pi$  coverage will maximize the angular coverage while minimizing the total surface area of the detector. In addition, the ability to use muon detection on opposite sides of the detector will allow rather accurate tracking through the central region without requiring high spatial resolution of the individual components.

At the far detector, the flexibility to construct a complete  $4\pi$  system is not available. The previously constructed laboratory is only big enough to allow the inner detector system. However, given that there is a significantly higher overburden at the far laboratory, the needs for large angular coverage and precise tracking are not as high. It is relevant, however, to be able to compare the effects of the veto system on data selection. We therefore envision placing a veto system in the access space directly above the far detector. This veto will be identical to the top component of the

$4\pi$  system at the near laboratory, thus providing comparable results. There will be an additional requirement that this veto at the far laboratory be movable to allow operation of the ceiling crane during periods of maintenance.

### 2.3.3 Detector Design

The muon veto will use gas-filled proportional chambers with a resistive wire for charge division. This will allow very efficient coverage of a maximum surface area while minimizing costs. The design is loosely based on the structures used in the Atlas muon chambers. It will be composed of a collection of 2 inch diameter aluminum extruded pipes with O-ring sealed end-plugs. A resistive wire will be strung down the middle, as shown in Fig 10.

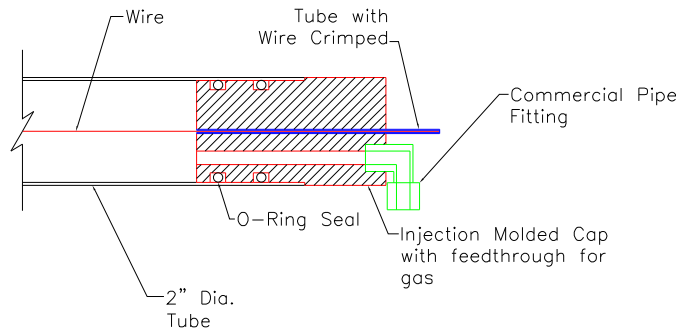


Figure 10: Schematic design of the veto chamber end-cap. The end-gap will be constructed of injection molded plastic with penetrations for the gas and wire feed-throughs. The end-cap will be double O-ring sealed against gas leakage and the resistive wire will be crimped in place under tension.

Since we expect to use charge division to identify the longitudinal position along the wire, full two dimensional tracking can be supplied with only a single orientation of the chambers. This greatly simplifies the mechanical construction. The Double-CHOOZ detector is cylindrical in shape so we have designed a system which is composed of a vertical barrel region capped by identical top and bottom planes.

The top and bottom planes will cover a 10m x 10m area. Each chamber will be 10m long and 80 of these will be epoxied together to create a module. The barrel region will be populated with vertical chambers in which a basic module will consist of 84 chambers (shown in Figure 11). As designed, the entire detector will be surrounded by 4 layers of proportional chambers. This should allow a high efficiency of muon detection while minimizing any impact from noise.

### 2.3.4 Electronics

The signals at each end of the proportional chambers will be summed together with 2 neighboring chambers to reduce the overall channel count. This signal will be immediately amplified and then transported to a standard VME crate. There the analog signal will be processed as shown in Figure 12: the analog signal is discriminated in a constant fraction discriminator which then latches a timestamp in a TDC. Then the charge is passed through a sample-and-hold integrator which is digitized by an 8-fold multiplexed ADC.



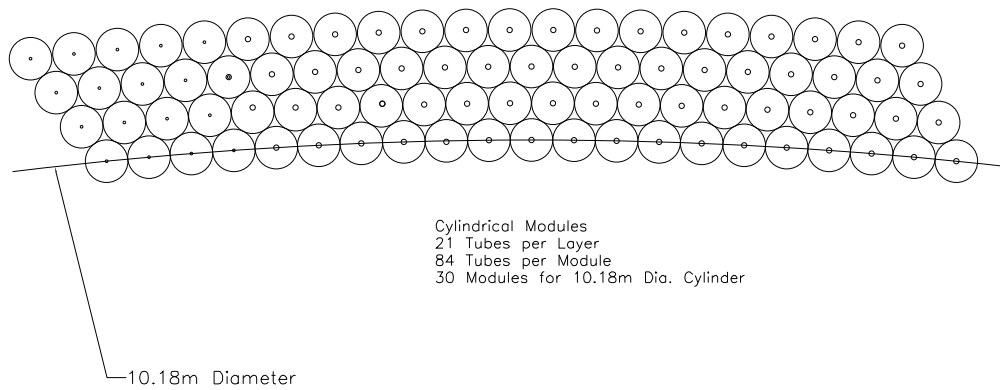


Figure 11: Schematic of a single barrel region module for the muon veto system. The 84 individual chambers will be epoxied together in the structure shown to exactly encircle the inner detector. The upper and lower planes will be similarly constructed out of 80 chambers and will be flat.

This design has the advantage of simplicity and self triggering, and should provide for sufficiently accurate time and position resolution. We expect that this system will have a maximum channel deadtime of  $100 \mu\text{s}$ . Previous experience with such chambers at Soudan [62] suggest that even above ground, a single tube rate of 100 Hz, dominated by local radioactivity, should be expected. The expected deadtime would not have a noticeable impact on this kind of signal rate.

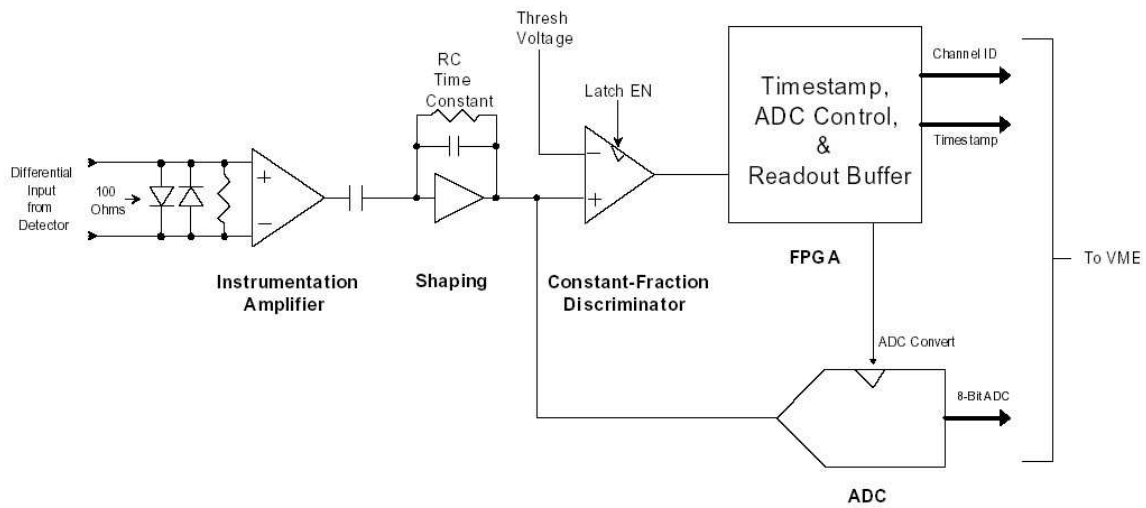


Figure 12: A schematic drawing of the expected electronics readout. The analog signals from the detector will be the sum of 3 neighboring chambers and will be amplified directly at the detector. The signals will then be transported differentially 10m to the VME racks where this system will be used to digitize any self-triggered signal.

## 2.4 Electronics

Figure 13 shows a schematic of the overall electronics organization for the Double-CHOOZ detectors. The main signal path is from the PMTs, through HV-splitters and front-end to a fast waveform digitization system where the pulses are recorded.

There will also be separate subsystems for providing high-voltage to the PMTs, a trigger, and extensive monitoring of detector operation.

### 2.4.1 HV-Splitters

The cable to the PMTs will be a single, high-quality cable suitable for oil-immersion. Such cable is expensive, and it is economically favorable to minimize the amount of such cable by using a single cable for HV and signal inside the detector, with a splitter to separate HV from signal at a point close to where the cable emerges from the detector.

In addition, the use of a single cable to the PMT greatly reduces ground-loop pickup which, since it occurs on all signal channels simultaneously, can be problematic for a detector where all PMTs are viewing the same event.

Figure 13 shows a schematic for a simple HV splitter. Although the HV splitter is in the signal path, it will be implemented as part of the HV system.

### 2.4.2 Front-End Electronics

The front-end electronics for the Double-CHOOZ experiment handles preamplification, producing analog sums of PMT signals for trigger and monitoring subsystems, pulse shaping and bandwidth limitation, baseline restoration and pulse distribution to other electronics subsystems.

Figure 14 shows a partial schematic for the front-end electronics. The front-end modules will be purely analog, to prevent any digital switching- or clock-noise pickup within the modules.

### 2.4.3 Trigger

Figure 15 shows a simplified schematic of the Double-CHOOZ trigger system.

The basic ('Level 1', or 'L1') trigger is a simple energy deposition trigger. In a detector of the Double-CHOOZ geometry with long attenuation length scintillator, the total light collected by the PMTs is a good measure of the energy deposition. While there are many ways to form an energy trigger from the PMT signals, a simple analog sum has the distinct advantage of being easily tested, calibrated and modeled. Other trigger options are also being explored as possibilities for the experiment.

Signals from the PMTs are fanned in, first in the front-end electronics, and further in the trigger system, with calibrated attenuation between fan-in stages to prevent electronic saturation. The final signal is then passed through a linear low-pass filter to minimize the effects of differing photon arrival-times at the PMTs.

Two discriminators are then used to define an energy threshold for L1 triggers and for 'muon' triggers.

The L1 trigger threshold will be set well below the minimum positron energy deposition, to obtain full efficiency for positrons produced in antineutrino interactions. The 'muon' trigger threshold will probably be at an energy deposition near 50 MeV. The L1 trigger will be sent to the waveform-recording electronics to cause the capture of information from all PMT channels.

The Level-2 ('L2') trigger is generated from having two L1 triggers occur within a coincidence time of  $200\ \mu\text{s}$ . This coincidence can be done either in hardware or in software, and a final implementation decision has not yet been made. An L2 trigger causes the readout of waveform information stored from the L1 triggers, possibly with extra L1 pulses that were prior to the L2 trigger, as an aid to background rejection.

Muon triggers, along with triggers from the veto system and calibration triggers, will also cause pulses to be stored and read out by the waveform system.

Since one of the major goals of the Double-CHOOZ experiment is to make the two detectors as identical as possible, the trigger thresholds must be set at the same energy. One way for this to be accomplished is to use a particular low-energy gamma source (such as  $^{137}\text{Cs}$ ) as a calibration standard for the energy threshold; this should allow the thresholds to be set at the same energy rather precisely.

#### 2.4.4 PMT rate monitor

The PMT rate monitor subsystem shown schematically in Figure 16 will be used to monitor the stability of the PMTs and associated electronics.

One of the most sensitive indicators of PMT gain stability is the single-photoelectron rate, so if that rate is stable it gives one confidence that the PMTs are indeed stable.

The PMT rate monitor will take fanned-in signals from the front-end electronics, discriminate the signals at a low (sub-photoelectron) level, then count pulses for fixed times to get a snapshot of the PMT rates.

The rate monitor could be implemented either with standard commercial discriminator and scaler modules, or with a simple custom design. Because the number of channels is moderate (approx. 600 per detector), it is not yet clear which approach is most cost-effective, but there should be no significant difference in performance.

In addition to the fanned-in PMT signals from the front-end, the rate monitor should also look at rates from the further stages of analog fan-in in the trigger, as well as the overall sums that are used for the triggers and vetoes. This will provide an end-to-end stability check for the analog electronics in the experiment.

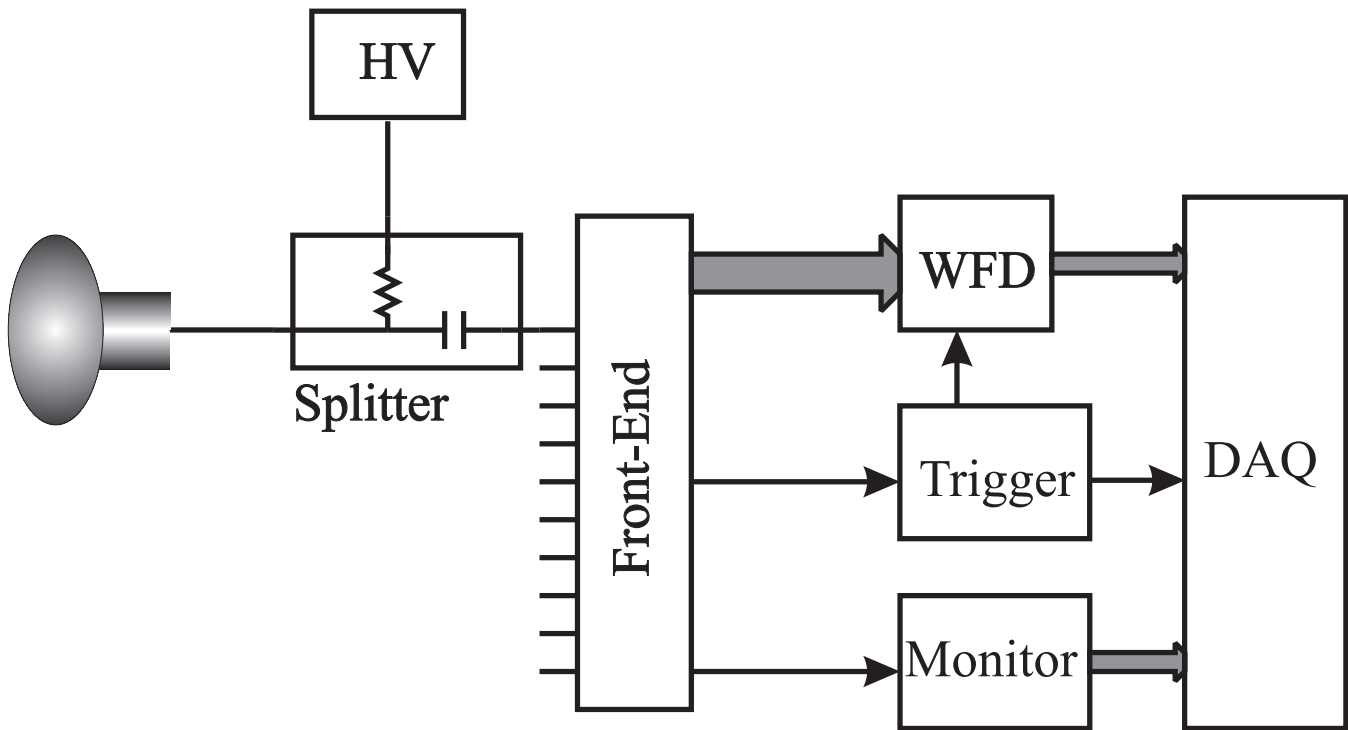


Figure 13: Block diagram of Double-CHOOZ electronics. The PMT signal and HV use the same cable within the detector, separated at the HV splitter. The analog front-end distributes the signal after (possible) amplification to waveform digitizers (WFD), trigger, and monitoring subsystems.

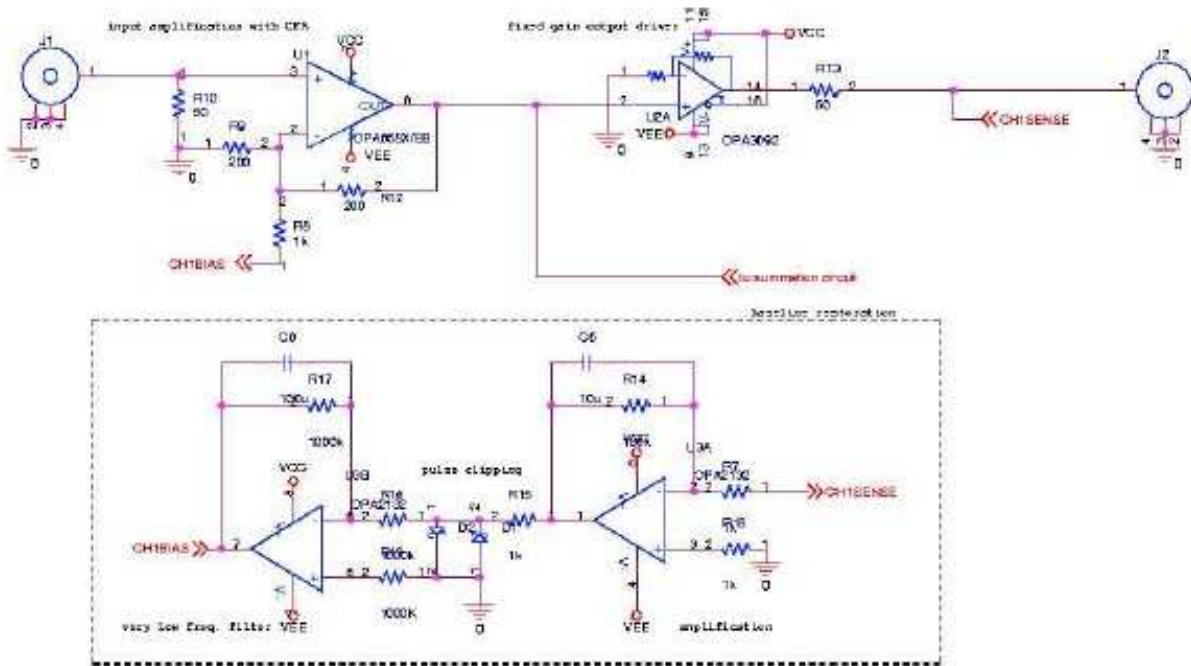


Figure 14: A partial schematic diagram for the analog front-end electronics. The use of DC-coupling in the signal path with baseline restoration avoids AC-coupling over-shoot for large (muon) signals, while minimizing DC offsets.

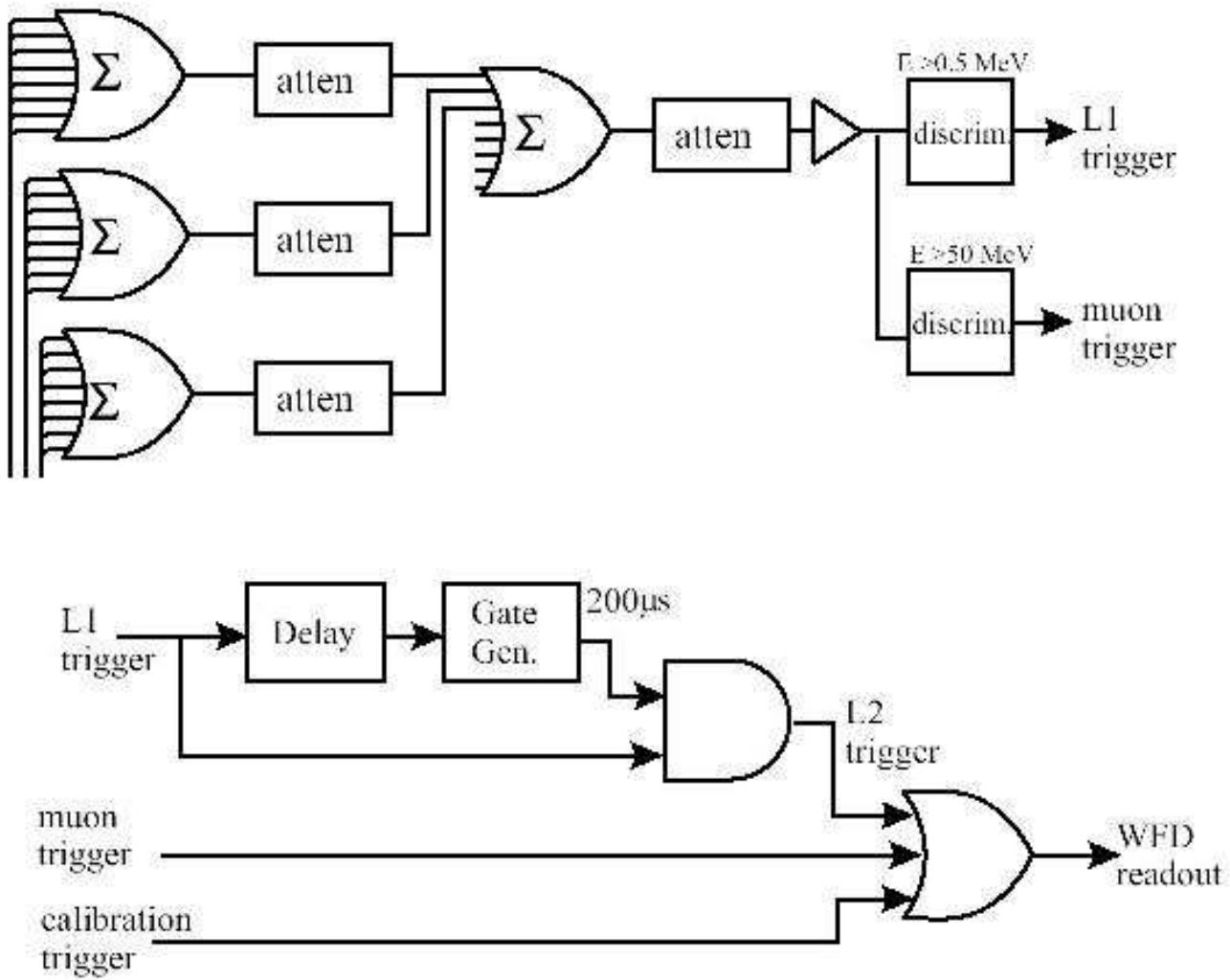


Figure 15: Block diagram for the Double-CHOOZ trigger system. The Level-1 (L1) trigger occurs when energy deposition is above 0.5 MeV. The Level-2 (L2) trigger occurs with a two L1 triggers within  $200 \mu\text{s}$ . Other triggers, such as a muon trigger ( $E > 50 \text{ MeV}$ ) and a trigger for calibration events, also cause WFD readout.

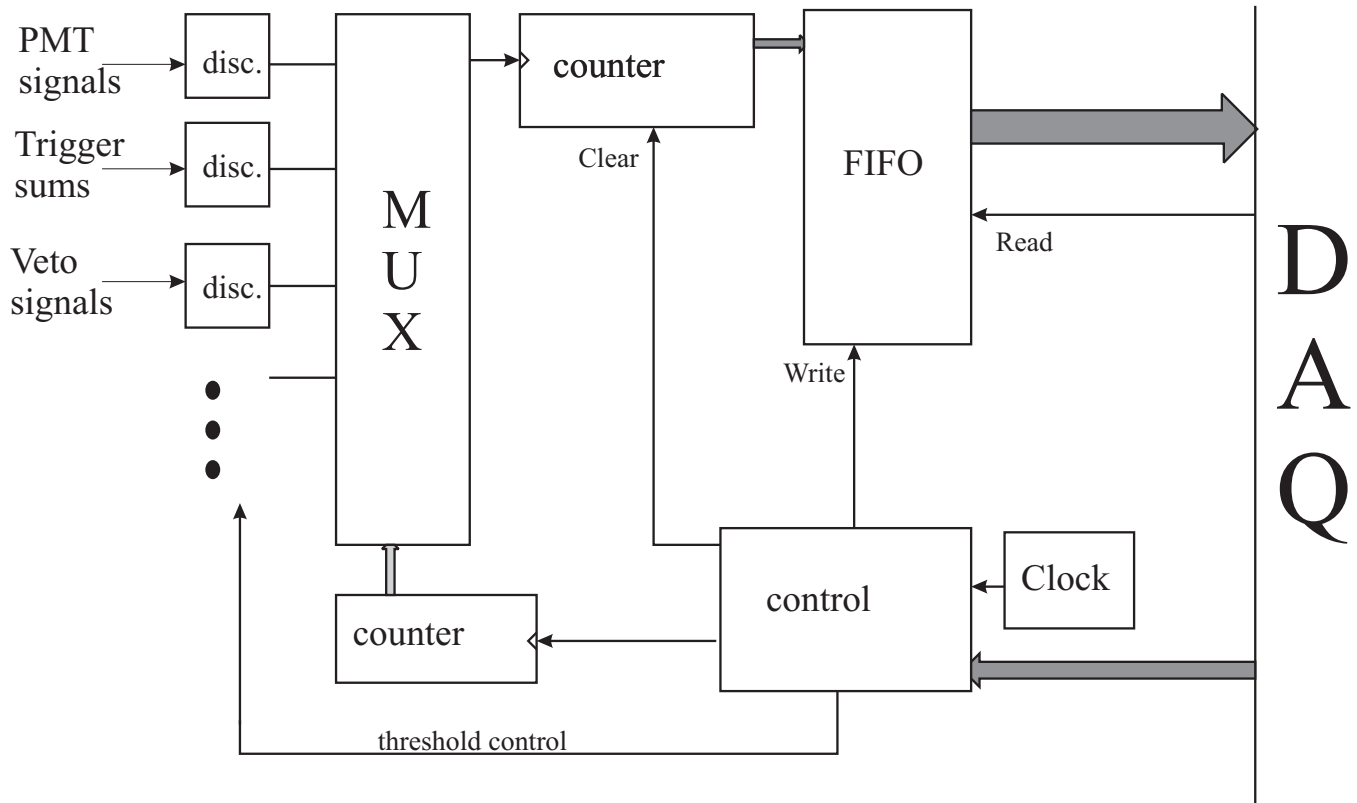


Figure 16: Block diagram of the PMT rate monitoring system. The monitor scans through PMT channels, counting single photoelectron pulses for a fixed time interval, and storing the rates for later readout. This subsystem can also monitor rates from the trigger system, providing a continuous check on the operation of the trigger.

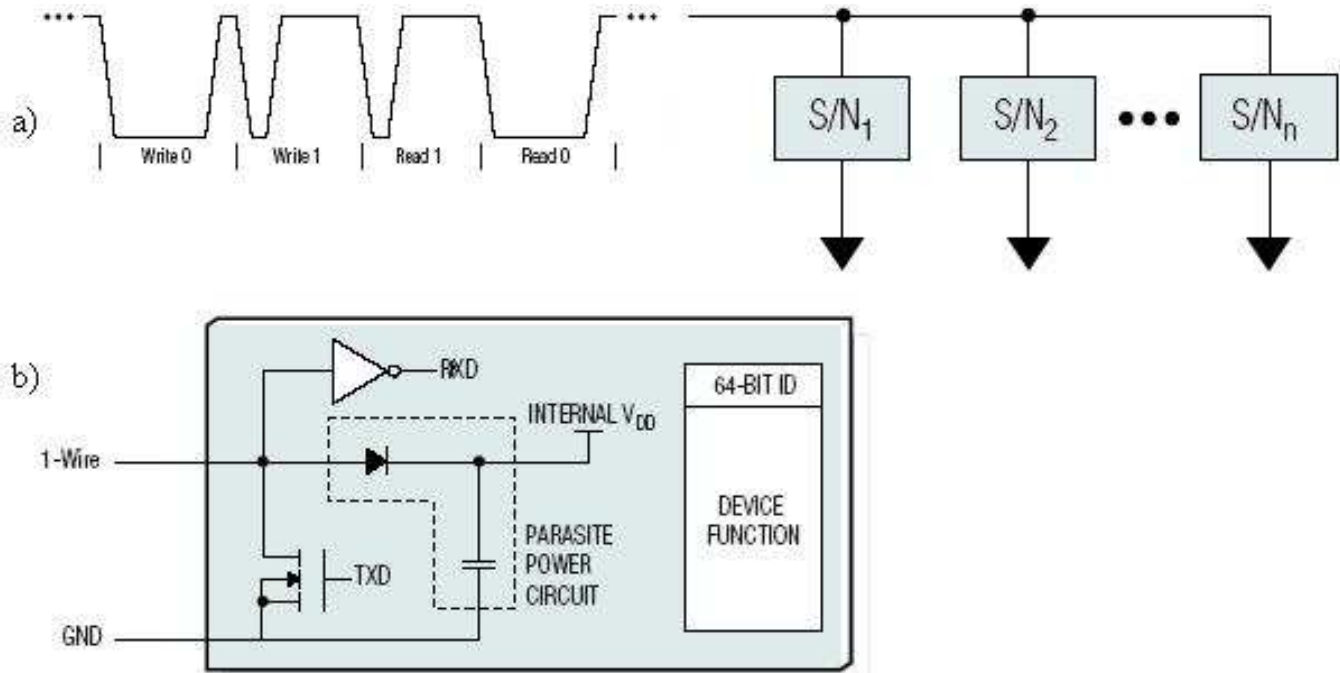


Figure 17: The 1-Wire<sup>®</sup> bus: (a) control, readback, and power provided to multiple devices over a “single” wire; (b) parasite power circuit captures power during high period of 1-Wire<sup>®</sup> waveform. (Adapted from figures by Maxim IC / Dallas Semiconductor.)

## 2.5 Slow Monitoring

A slow monitoring and control system is required to control systematic effects that could impact the experiment, to allow automated scans of parameters such as thresholds and high voltages, and to provide alarms, warnings, and diagnostic information to the experiment operators. The quantities to be monitored and controlled include temperatures and voltages in electronics, experimental hall environmental conditions, line voltages, liquid levels and temperatures, gas system pressures, radon concentrations, photo-tube high voltages, and discriminator settings and rates. Most of these functions can be accomplished using “1-Wire<sup>®</sup>” devices from Dallas Semiconductor [63]. The high voltage and discriminator subsystems will have their own control and readback hardware. All slow monitoring and control systems will use the same database and history log software. A computer in each experimental hall will monitor the local 1-wire bus and a local radon monitor, acquire any data provided by other subsystems, record the data, and make the data available via the local internet connection.

### 2.5.1 Monitoring via 1-Wire interface

The “1-Wire<sup>®</sup>” line of semiconductors from Maxim IC / Dallas Semiconductor use a simple interface bus that supplies control, readback, and power to an arbitrary number of devices over a single twisted-pair connection [63]. (Figure 17.) A variety of sensor and control functions are available in traditional IC packages and stainless-steel-clad “iButton<sup>®</sup>s”. (Figure 18.) Each device has a unique, factory-lasered and tested 64-bit registration number used to provide device identification on the bus and to assure device traceability. Some devices are available in individually calibrated



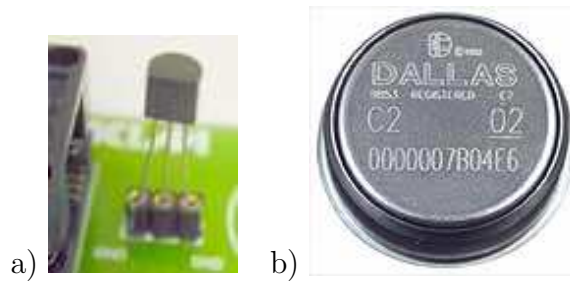


Figure 18: Examples of 1-Wire<sup>®</sup> devices: digital thermometer in (a) TO-92 package and (b) iButton<sup>®</sup> case, 17.35 mm in diameter. Figures are not shown at the same scale. (From Maxim IC / Dallas Semiconductor web site [63].)

NIST-traceable packages. The features of low cost, multidrop capability, unmistakable device ID, and versatility make this an attractive choice for implementing the slow instrumentation and control system.

Implementation details and expected performance for several subsystems are given here.

**Crate and card temperatures and voltages:** Temperature and voltage monitoring can be included in any custom-built electronics at a component cost of only a few dollars per device using DS18S20 and DS2450 chips and low-cost modular connectors to connect to the 1-Wire<sup>®</sup> bus. Note in addition to the temperature and voltage functions, the unique ID on each chip provides automatic tracking of any card swaps. Trivial custom boards containing only these components can be used to monitor temperature and bus voltages on crates which otherwise contain no custom-built electronics.

In these chips, digitization of temperature and voltage is initiated by an explicit “convert” command from the bus master. Temperature conversion takes 900 ms, and digitization of the four 12-bit channels of the DS2450 takes less than 4 ms total. During conversion, the bus master may communicate with other devices if the chips have an external source of power; if a chip is powered parasitically from the bus, then the master must maintain the bus level high throughout the conversion. Testing of samples provided by Maxim IC / Dallas Semiconductor confirm that multiple devices can maintain their internal state while all are powered parasitically from the same bus. Figure 19 shows data from a three day period during which two DS18S20 thermometers were sampled once a second by a program written in Java. The two thermometer chips were mounted in direct contact with each other, and recorded the same temperature to within a small fraction of a degree. In this test, the thermometers were located about two meters from the bus master, and another 1-Wire<sup>®</sup> device was connected on the same bus about three meters further downstream. No failures or interruptions occurred during this period.

**Experimental hall environment:** The DS1923 “Hygrochron” iButton<sup>®</sup> looks ideal for monitoring temperature and humidity. In addition to the humidity and temperature functions, this device features on-board battery backup and automatic logging to internal memory independent of external control. Power or computer failures will not interrupt the temperature and humidity record. This iButton<sup>®</sup> is designed for tracking sensitive products during shipment or other handling. Each DS1923 is individually calibrated and NIST traceable. Another iButton<sup>®</sup>, the DS1922, provides similar functionality without the humidity function.

Monitoring of barometric pressure and other environmental factors is easily achieved using the DS2450 ADC and one or more external transducers. (Note: A complete 1-Wire<sup>®</sup> weather station

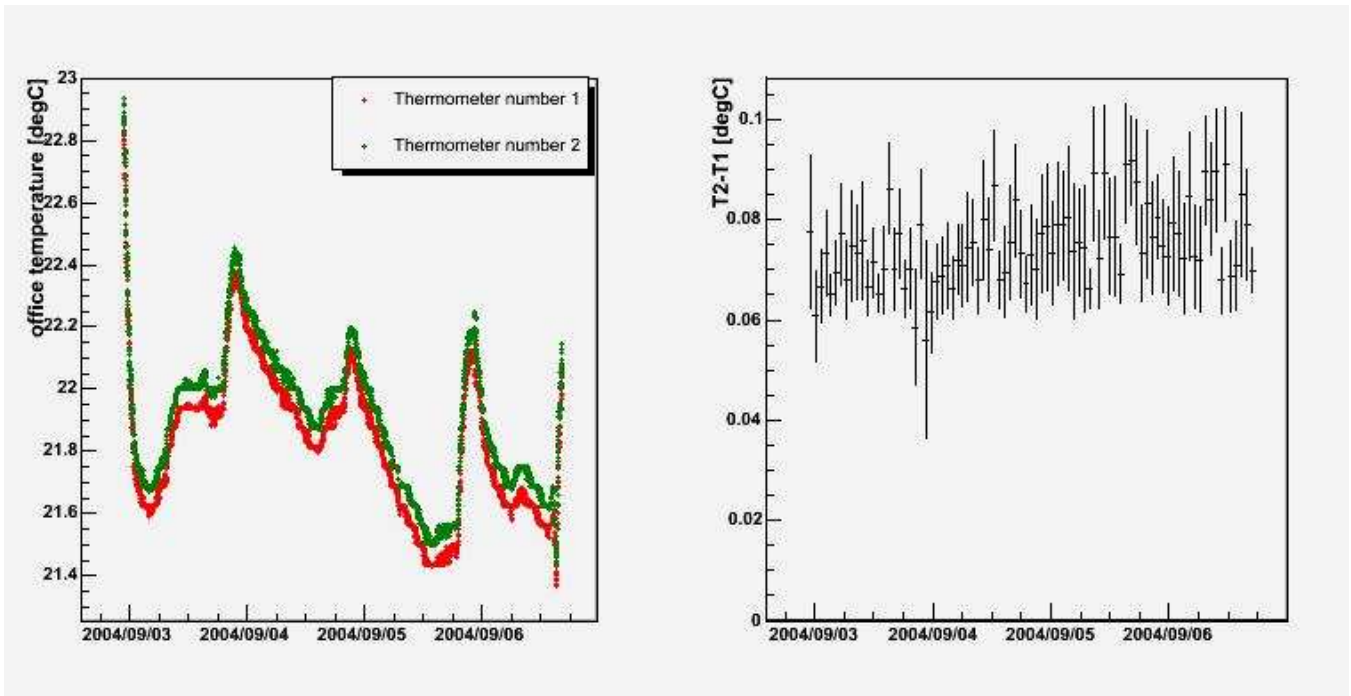


Figure 19: Data from three day test of several 1-Wire<sup>®</sup> samples: (a) temperature in an office at Kansas State University vs. time as read by two adjacent DS18S20 thermometer chips; (b) difference in reading of the two chips.

is even available [64].) Another interesting “environmental” condition to monitor is ambient light level in the experimental area: many systematic effects in past and present neutrino experiments have been attributed, correctly or incorrectly, to electrical or optical noise introduced by lighting, and a simple phototransistor addresses the issue handily. The phototransistor technique also can be used to monitor status LEDs on devices which lack electrical status outputs. AC line voltage is also easily monitored using a 1-Wire<sup>®</sup> ADC and a trivial circuit.

**Liquid levels and temperatures, and gas pressures:** Transducers should be provided for monitoring important aspects of the detector such as scintillator and buffer oil levels, temperatures, and pressures in any gas systems used. Transducers should produce voltages in the 0 to 5 V range for maximum compatibility with the DS2450 ADC. The further specification, purchase, and installation of such transducers are the responsibility of the respective subsystems.

**Simple controls:** The DS2890 is a 1-Wire<sup>®</sup> digitally controlled potentiometer. It can be used to provide slow control for simple servos, power supplies, or other devices controllable by an external analog signal. At present, there is no definite plan to use this capability, although the discriminator levels could possibly be controlled in this way. Support for slow control as well as monitoring should be provided in the software for maximum flexibility.

### 2.5.2 Radon monitoring

Professional continuous radon monitors have become readily available and relatively inexpensive. An example is Sun Nuclear’s Model 1027 [65]. Each experimental hall will have at least one radon monitor read out by the slow control PC. The data will be stored and made available via the same

interface used for all slow monitor data.

### 2.5.3 Interface to other subsystems

Some hardware subsystems may have important slow monitor data that cannot be made available on the 1-Wire<sup>®</sup> interface or the serial ports of the slow monitor computers. Examples may include the clean room particle counters, the high voltage power supplies, and the discriminator circuitry in the trigger system. In such a case, either the hardware itself or a computer which monitors and controls it should make the data available via network TCP connection. “Virtual” monitor data, such as capture time, event rates, or other quantities determined by online analysis, could also be recorded by this mechanism. The software on the master slow monitor computers will poll these external servers and make all slow monitor data available in a common framework. This is preferable to each subsystem providing a separate data interface. In the common framework, systematic correlations may be studied among any variables. Support for control functions and synchronization with externally controlled devices should be provided in the software to allow for scans of controlled parameters such as high voltages and threshold levels. The common framework will allow dependent variables observed in one subsystem, *e.g.*, discriminator rates, to be easily correlated with parameters monitored or controlled by some other subsystem, *e.g.*, high voltage.

## 2.6 Laser System

The laser calibration system proposed here is based on the experience with the similar systems that have been employed successfully within the LSND, MiniBooNE, CHOOZ, and KamLAND experiments. The primary purpose of this system is to quantify and monitor pertinent properties of each individual PMT: PMT gain, relative quantum efficiency, pulse-height versus photoelectron linearity, and timing. Other functions of the system include the measurement and monitoring of the attenuation length of the scintillator over the lifetime of the experiment, and the reconstruction of the light source locations. In addition, this will be a valuable tool for commissioning the detector and data acquisition testing.

The system will consist of a short-pulsed laser and a light distribution module which transmits the light through quartz optical fibers to a diffuser ball which can be positioned anywhere throughout the fiducial volume with the calibration deployment system. The possibility of permanently deploying laser balls for monitoring purposes is being considered. Using a laser of wavelength within the absorption band of the scintillator the light emitted by the scintillator-filled dispersion laser balls will have the same characteristics as the scintillator light. The intensity of the laser light can be modulated via a system of computer-controlled attenuator wheels.

The laser system will be operated by a stand-alone control system running a real-time control program on a dedicated PC and could operate at a rate of up to several tens of Hz. A reference photo-diode would provide a tag signal for the data acquisition system for each laser firing. The single PE response, relative quantum efficiencies, and gain calibrations can be obtained from low intensity, low frequency background runs using the laser ball positioned at the center of the detector. Special calibration runs with high intensity light levels determine uniquely the time offsets of the PMTs. Time slewing corrections are determined from laser calibration runs covering all intensities.

## 2.7 Calibration Deployment

### 2.7.1 Introduction

The purpose of the calibration deployment system is to deploy calibration sources into the target and gamma catcher regions. The calibration sources and the motivation for using them have already been described above. The deployment systems utilized by the near and far detectors will be identical.

The U.S. Double-CHOOZ collaboration has experience in the design and operation of calibration source deployment systems, most notably for KamLAND but including also Super-Kamiokande, K2K, and Palo Verde.

Calibration sources which the deployment system must be designed to accommodate include point gamma sources, terminated fibers illuminated by external lasers, and neutron sources. These characteristic dimensions of these source will range from a few mm to a few cm, and the masses of the sources will range from a few tens of grams up to a few hundreds of grams. The calibration system must be capable of positioning sources within every representation region of the target and gamma catcher with an uncertainty which is small compared to the intrinsic vertex resolution of the detector in the energy range of 1–8 MeV; a deployment system with a positioning accuracy better than 2.5 cm will satisfy this requirement.

The materials and geometry of the deployment system must be chosen to minimize uncertainties in the corrections for shadowing and absorption. Neither the materials of the deployment system itself, nor the process by which deployment system introduces calibration sources into the detector can measurably increase detector backgrounds or affect detector performance. Setup of the deployment system for inserting a particular source into the detector cannot be awkward or time consuming and calibrations which are carried out frequently should be largely automated.

In what follows, we describe in the deployment system in 3 parts: (1) deployment methods, (2) detector interface, and (3) control systems.

### 2.7.2 Deployment Methods

The methods of source deployment for the target region will be different from that of the gamma catcher region because of the different geometries and different calibration requirements, therefore, they are discussed separately.

#### Target

The complete set of calibration sources must be deployable throughout the representative target regions because the experiment intends to use the complete target volume as the fiducial volume. (Recall from Section 1 that the target is cylindrical with a height of 2.8 m and a diameter of 2.4 m; the center of the target is about 3.5 m below the top of the detector.) Two design options are being considered to realize this capability, a cable-and-pulley system in two orthogonal planes and an articulated arm. The deployment system will access the target through a vertical tube from the detector interface. Actuators, as well as sensors for determining the deployment system position, would be located on the deployment system and in the detector interface. For the option of an articulated arm, given that the distance from the top of the inner veto to the bottom of the target is about 5 m, mechanical members comprised of thin metallic tubes or transparent plastics should suffice to provide adequate stiffness while minimizing absorption and shadowing. During a calibration, an operator would attach a calibration source to the source holder, deploy the source into

the target at the desired positions, and then retract the source to the detector interface. The design and operation of the deployment system must take into account permanently mounted calibration sources, if any, in the target region.

In addition to a cable-and-pulley system or an articulated arm, a simple winch system will be used to deploy sources along the symmetry axis of the target. With this system, a small subset of calibration sources can be quickly deployed on a frequent basis for the purpose of monitoring detector stability. The results of source calibrations on the symmetry axis will be used to determine when it is necessary to repeat a full calibration of the target and to interpolate the detector calibration between the full calibrations.

Those components of the deployment system which come in direct contact with the scintillator will be checked for compatibility. Compatibility tests will include soaking in liquid scintillator and then checking soak scintillator samples for changes in light yield, transparency, and radio-contamination. Components that will not come into direct contact with the scintillator but which will be exposed to its vapors must also be tested. After the first round of design is complete for the cable-and-pulley system or the articulated arm, a system prototype will be built and tested in air or water. All components of the deployment system will be carefully cleaned before installation into the experiment.

### Gamma Catcher

The gamma catcher requires its own calibration because its light yield and properties of light and neutron transport will likely differ from that of the target. These differences can be measured using gamma and neutron sources.

To deploy sources in the gamma catcher, a set of guide tubes is being considered. These tubes would be transparent and small to avoid shadowing of scintillator light and to minimize dead material and absorption. Most tubes would run from a manifold in the detector interface to insertion points at the top of the gamma catcher. The calibration sources would be attached to a cable and inserted into a tube. The tube would then guide the source to the top of the gamma catcher, from which the source would lower vertically into the gamma catcher region as additional cable is pushed into the tube. Whether or not additional guide tubes running through the gamma catcher to position sources in its top or bottom regions are needed is being studied. The position of the source can be determined from the length of cable inserted into the tube and an accurate survey of the guide tube geometry. A guide tube system was used in the Palo Verde experiment to deploy sources with a precision of 2 cm over distances ranging up to 14 m. Following the same practice as for the target, a small subset of sources would be deployed frequently to monitor stability.

A minimum of 6 guide tubes at three azimuthal positions and two radii would be installed. The connection of the cable to the sources should be such that the same sources can be deployed in the gamma catcher as in the target. As with the deployment system for the target, all components would have to be checked for compatibility before final selection and carefully cleaned before installation into the experiment.

### **2.7.3 Detector Interface**

The detector interface is the region which has access to the target and gamma catcher and which can be accessed from the outside to introduce and remove calibration sources. The volume of the detector interface has to be large enough so that sources can be easily manipulated and the deployment system can be assembled and disassembled as needed safely and easily. It must be

connected to the experiment gas system and purged so that, when it is opened to the detector, it has the same atmosphere to avoid introducing backgrounds. The glovebox will be equipped with radon and oxygen monitors for flagging leaks and monitoring the progress of purging. While the detector interface is open to the detector, it must also be light tight, which may mean that the operator must view the interior of the glovebox using infrared illumination and cameras. Feedthroughs for laser fibers and control and power cables must be hermetic. To bring sources into the detector interface, a transfer box is needed: sources are placed into this box through an external door, then the the transfer box is purged, after which the operator opens an internal door and brings the source inside the detector interface.

Most likely, the detector interface can be built by modifying a commercially available glovebox. The mechanical design of the detector will provide a defined set of flanges and supports for the detector interface so that the design of the interface and deployment systems can be largely decoupled from the design of the rest of the detector.

#### **2.7.4 Control Systems**

All control and sensor channels for the deployment systems should be interfaced to a computer system for the purpose of automation and ready monitoring. Although it should be possible to monitor the state of the deployment system remotely, for safety and convenience, the computer system providing control as well as monitoring of the deployment system should be installed near the deployment interface. Interlocks, both hardware and software, must be implemented to ensure that the detector is not opened to light, that a valve between the detector interface and the detector is not closed while sources are being deployed, etc. Full exercise of the control program and interlock system will be part of the testing of the deployment systems.

## 2.8 Radiopurity maintenance

A system is needed to exclude dust, radon, and radioactive krypton-85 present in the air from entering the active volume during detector operation. Given the anticipated rate of untaggable external neutron captures in the central volume [66], we require a rate under 3 Hz of singles exceeding the prompt energy analysis threshold in order to keep accidental backgrounds under control. This requirement is relatively weak in comparison to the requirements met successfully by KamLAND and Borexino's Counting Test Facility, but is still strict in comparison to what can be expected in scintillator casually exposed to ordinary air, for reasons explained below.

The US groups will work closely with European collaborators to develop suitable systems to establish and maintain scintillator radiopurity. These systems should include a clean room around the calibration access ports, a clean calibration source preparation facility, and a radon- and krypton-free nitrogen blanket to isolate the scintillator from the air during normal operation and source deployment.

### 2.8.1 Potential for contamination from $^{222}\text{Rn}$ , $^{85}\text{Kr}$ , and dust

The average concentration of radon ( $^{222}\text{Rn}$ ) in fresh outdoor air is about 0.4 pCi/L (15 Bq/m<sup>3</sup>). Indoors, particularly in underground structures, the radon concentration can be from one to several orders of magnitude higher. The relative solubility factor for radon in mineral oil relative to radon in air is about 10 [67], so exposing a large surface area of the scintillator to air would result in thousands of Becquerels of radon activity in the active volume.

In actuality, all but a small area of the scintillator is protected from the air. Because the liquid in the chimney is usually fairly static, and the diffusion constant of radon in organic liquids is generally a little less than  $3 \times 10^{-5} \text{ cm}^2\text{s}^{-1}$  [67], a layer as thin as 10 cm is sufficient to limit the radon diffusion into the central volumes to acceptable levels. However, during source deployment, the liquid in the chimneys is disturbed, and some scintillator from the top of the chimney may be brought into the fiducial volume. In the event the top of a calibration chimney were in direct contact with lab air with a modest radon concentration of 100 Bq/m<sup>3</sup> (below EPA's recommended action level), as little as a liter of scintillator from the top of the chimney dragged into a central volume would cause a significant and unacceptable increase in the singles rate.

A similar situation exists with respect to the radioactive noble gas  $^{85}\text{Kr}$ , produced by fission reactions and emitted especially during reprocessing activities, such as those performed at the nearby La Hague reprocessing plant. Atmospheric concentrations of  $^{85}\text{Kr}$  are typically at the 1 Bq/m<sup>3</sup> level [68], but measurements made at Gent, Belgium, show that sudden jumps of many orders of magnitude often occur [69]. The relative solubility of krypton in organic liquids is about 1. When atmospheric  $^{85}\text{Kr}$  levels are at their lowest, their potential for contributing activity to the scintillator is therefore two or three orders of magnitude less than that of radon; however, when atmospheric  $^{85}\text{Kr}$  levels are high, they could dominate over radon. It should also be noted that the  $^{85}\text{Kr}$  spectrum contributes primarily to the lowest energy bins, thus concentrating the activity in a part of the spectrum we would like to use for measuring background.

The activity and concentration of dust may vary from one laboratory to another. To get an idea of the risk posed by dust, we consider the experience of the SNO experiment [70]. They maintained "class 2500  $\pm$  500" cleanroom conditions throughout the experimental area, and attained deposition rates of 300  $\mu\text{g}/\text{cm}^2/\text{month}$ . An open 20-cm-diameter calibration port would thus collect a few micro-Becquerels per month of uranium, thorium, or potassium under these conditions. However,



particulate levels in ordinary, non-cleanroom areas may reach an equivalent of “class 400 million” [71], over one hundred thousand times as high as those seen in SNO. Scaling from the SNO experience, we see the potential for a few tenths of a Becquerel per month to be deposited in the scintillator if no precautions were to be taken to avoid it. Trivial measures such as keeping the ports covered when not in use may not be enough to prevent contamination on the order of a few Becquerels over the life of the experiment.

### 2.8.2 Control measures

Several measures should be taken to avoid contamination by dust, radon, and radioactive krypton-85. The calibration ports should be kept closed when not in use. The space between the top of the liquid and the chimney covers should be flooded with pure nitrogen. The nitrogen should have less than 0.1 Bq/m<sup>3</sup> of radon and <sup>85</sup>Kr. The air around the calibration access ports should be kept at class 10,000 or better. Calibration sources will be cleaned and prepared as described elsewhere in this document; after cleaning, it should be possible to bring them to the clean deployment area without exposing them to unclean air. Radon levels in the area around the calibration chimneys will be monitored as described in the slow monitoring section of this proposal. We will investigate the possibility of obtaining estimates or forecasts <sup>85</sup>Kr levels from European authorities or monitoring it ourselves. With these precautions in place, the cleanliness requirements for this experiment should be easily met.

## 3 Cost and Schedule

### 3.1 Overview of Costs

At the Chooz site, the laboratory previously used by the CHOOZ experiment is vacant and available as a far site for use with minimal preparation. Electricite de France (EdF) made a major contribution to the CHOOZ experiment in constructing the laboratory, and has been asked to contribute to Double-CHOOZ by constructing the near detector laboratory. The relationship between the CHOOZ experiment and EdF was very cooperative and cordial; the success of a  $\theta_{13}$  experiment such as Double-CHOOZ requires such close cooperation. We are optimistic that EdF will again be a willing partner in cutting-edge neutrino science.

The current estimate for the cost of both detectors, (not including the near detector lab) is 9.0-9.5 million euros. In France, IN2P3 and CEA/Saclay have approved a contribution of 2.2-2.5 million euros. proposed contributions from Germany and the other collaborators are in the early stages of the funding process. The CHOOZ-US collaborators are requesting \$4.858M as detailed in Section 3.4, primarily for phototubes, electronics and an outer veto system for the near detector. These crucial parts of the experiment coincide with the expertise of the U.S. collaborators, who have extensive experience not only in phototubes, but also in high voltage and front-end electronics, laser calibrations, deployment systems, and muon tracking systems.

### 3.2 Overview of Schedule

The anticipated schedule calls for the completion of an R&D phase in 2004 followed by project definition. This will include a prototype to evaluate technical solutions. Production phase would be February 2005-October 2007, with the far detector completed in October 2007. The construction of the near detector is scheduled to be completed in March 2008. Detector operations would be for three years, 2008-2011.

First results are in principle possible with just the far detector because the luminosity of the important original CHOOZ experiment will be matched in just a few months. Using both detectors, Double-CHOOZ will reach a sensitivity  $\sin^2(2\theta)$  of 0.05 in 2009 and 0.03 in 2011. Whether running any longer at that time makes sense will depend on an evaluation of systematic errors and backgrounds achieved to date, as well as the world situation regarding  $\theta_{13}$ .

Photomultipliers and the high voltage system would be returned to the U.S. after the experiment is over.

### 3.3 Work Breakdown Structure (WBS)

The CHOOZ-US scope, consisting of cost, schedule and an understanding of US participation, is driven by the European project completion date of April 2008. Provided here is a description of US scope delineated by work elements, a description of those elements, the cost structure for those elements, escalation considerations, and a schedule to meet Double-CHOOZ goals.

#### 3.3.1 Work Breakdown Structure Description

The following describes US contributions to the Double-CHOOZ project. These contributions provide essential components, functionality, and assured integration of US and European systems. They

form the foundations of work packages used to track schedule, cost and deliverables. The WBS is organized in six major work packages. Work is further resolved into ensuing levels until reasonable details are addressed. This structure becomes the cost and schedule template for the conceptual design cost estimate. The major Double-CHOOZ WBS follows:

1. Inner Detector
2. Outer Detector
3. Signals and Processing
4. Calibration
5. Management and Common Projects

A terse description is provided for second level WBS elements which are part of the US project scope.

### 1.3 PMTs

Provides for the System of phototubes for the near detector target, and the the far detector target. Provides for the purchase of 1050 photomultipliers. 16 spares are included. The tube is the 8 inch ETI 9354, Hamamatsu R5912, or similar low-background PMT. We have used a quote from Hamamatsu as the basis for costing the PMT, PMT base electronics, potting, and under-oil cable. Quality Control Checkout, DOE tagging and inventory will be performed at Louisiana State University. Phototube purchasing will be done by Louisiana State University and task progress will be monitored by Argonne National Laboratory. A structure inside the detector(s) for mounting and installing the phototubes will be developed at the University of Alabama.

### 2.2 Outer Veto

Provides a system of 5000 gas proportional chambers for the identification of muons in the near detector and to veto associated background events. This requires the design of modular assemblies of the proportional chambers as well as the associated electronics, gas and support systems. After the completion of technology testing and design reviews, procurement and production will be shared between Argonne National Lab and the University of Tennessee. Argonne National Lab will be responsible for progress monitoring and reporting as well as supervision of final shipment and installation at the experimental detector laboratories.

### 3.1 Analog Front End Electronics

Based on requirements for 1024 phototubes, provides for the electronics for readout of all phototubes in the near and far Double-CHOOZ detectors plus 20% spares. Includes design and engineering of preliminary and final designs, Preliminary Design Reviews (PDR) and Final Design Reviews (FDR), component monitoring, coordination of the generation of software with the project scientific staff, all testing and supporting documentation and operating manuals. It will include assembly and testing at Drexel and installation at the near and far detector laboratories for Double-CHOOZ in France. The front-end electronics task at Drexel University will use existing graduate student RA and travel support at approximately 2/3 FTE level, as the Drexel group makes the transition from KamLAND to Double-CHOOZ over the next two years, however some additional operations funding is included here as necessary for the Double-CHOOZ effort.

### 3.4 High Voltage

Based on requirements, provides for a single system for high voltage supply to all photomultiplier tubes. Two primary candidates for HV systems are Connecticut-based Universal Voltronics and CAEN from Italy. Cost quotations from both are in hands. This item provides for 1024 channels. DOE tagging and inventory will be performed at the University of Tennessee. This contract will be monitored by Argonne National Laboratory. Quality assurance, cabling, testing, installation, and maintenance of the high voltage system will be provided by the University of Tennessee.

### **3.5 Slow Control and Monitoring**

Based on requirements, provides a system to control and scan items such as thresholds, high voltage settings and temperatures, and to provide alarms, warnings and diagnostic information to the experiment operators. This provides for the purchase from Maxim IC/Dallas Semiconductor 1-Wire interface chips and other components needed to control and readback hardware. Assembly will take place at Kansas State University and Installation at the Double-CHOOZ laboratories in the Ardennes region of France. The PMT monitoring is to provide periodic samples of PMT singles rates at a sub-photoelectron threshold, with readout and alarm software integrated into the main DAQ. Assembly and testing will be performed at Drexel University, and installation at the Double-CHOOZ laboratories.

### **4.2 Mechanical Deployment of Sources in 3 dimensions**

Provides for the accurate deployment of calibration sources within the target and gamma catcher regions of the detectors. The development and assembly will be done by the University of Alabama, with assistance from the Argonne National Lab for mechanical engineering.

### **4.3 Laser System**

Provides for a laser system to quantify and monitor pertinent properties of each photomultiplier. The system will be developed and tested at the University of Alabama and installed in the Double-CHOOZ laboratories.

### **5.1 & 5.3 Project Coordination, Engineering Coordination**

Consists of tasks which are the responsibility of CHOOZ-US project engineer at Argonne National Laboratory. Includes project engineering. Systems engineering and integration will be responsible for defining interfaces, pre-installation logistics and installation logistics and day-to-day communications with European Collaboration counterparts.

### **5.2 & 5.4 Technical Direction and Cost and Effort Monitoring**

Consists of CHOOZ-US management at Argonne National Laboratory. Includes administrative tasks in accordance with the management plan. Documentation and performance tracking will be the responsibility of the Project Manager.

### **5.5 Progress Monitoring and Reporting**

Provides for administrative expenses involved with quarterly reporting of progress on costs and schedules to the Department of Energy.

### **5.6 Shipping**

Shipping involves transportation expenses for final components of US systems from Argonne to the Double-CHOOZ site in the Ardennes region of France.

### 3.3.2 Full WBS

The Full Work Breakdown Structure is as follows:

1. Inner Detector
  - 1.1. Vessel Mechanics
  - 1.2. Liquid Scintillator
  - 1.3. PMTs
    - 1.3.1. PMT Procurement
    - 1.3.2. Dark Box Construction
    - 1.3.3. Checkout and testing of PMTs
    - 1.3.4. Mount and Assembly of PMTs
2. Outer Detector
  - 2.1. Inner Veto
  - 2.2. Outer Veto
    - 2.2.1. Design of Modules and Fixtures
    - 2.2.2. Module Factory Setup and Tooling
    - 2.2.3. Component Procurement
    - 2.2.4. Module Assembly and Repair
    - 2.2.5. Wire Stringing
    - 2.2.6. Module Testing
    - 2.2.7. Design of Support System
    - 2.2.8. Support System Construction
    - 2.2.9. Design of Gas Systems and Prototype Testing
    - 2.2.10. Gas System Construction
    - 2.2.11. Electronics Design and Prototype
    - 2.2.12. Electronics Small System Test
    - 2.2.13. Electronics Production
    - 2.2.14. Supervision of Installation on site.
3. Signals and Processing
  - 3.1. Analog Front End Electronics
    - 3.1.1. Electronics and Trigger Design and Prototype
    - 3.1.2. Components
    - 3.1.3. Assembly and Testing
  - 3.2. Digital Electronics
  - 3.3. Data Acquisition System
  - 3.4. High Voltage
    - 3.4.1. High Voltage Power Supplies
    - 3.4.2. High Voltage System Components
    - 3.4.3. Design, Assembly and Installation
  - 3.5. Slow Control/Monitoring
    - 3.5.1. Slow Control Components
    - 3.5.2. Slow Control Design, Assembly, Installation and Travel
    - 3.5.3. PMT monitoring Design and Prototype
    - 3.5.4. PMT Monitoring Assembly and Installation
4. Calibration
  - 4.1. Radioactive Sources

- 4.2. Mechanical deployment of sources in 3-dimensions
  - 4.2.1. Engineering Design
  - 4.2.2. Target System Fabrication/Assembly/Testing
  - 4.2.3. Gamma Catcher System Fabrication/Assembly/Testing
  - 4.2.4. Shipping Travel and Installation
- 4.3. Laser System
  - 4.3.1. Laser Head, Driver and Switch Box
  - 4.3.2. Installation and checkout
- 5. Management and Common Projects
  - 5.1. Project Coordination
  - 5.2. Technical Direction
  - 5.3. Engineering Coordination
  - 5.4. Cost and Effort Monitoring
  - 5.5. Progress Monitoring and Reporting
  - 5.6. Shipping to Experiment Location

### **3.4 Cost & Schedule Details**

The cost estimation for the CHOOZ-US project was made on the basis of the specific requirements for each WBS system. The estimates were generated by specific engineers or supervising physicists with previous experience from other similar projects. Where possible, commercial vendors and catalog information was used for costs related to materials and sub-contracted services. The following assumptions were made:

1. US systems will not be subject to any taxes or tariffs for shipping and installation at the experimental site in France.
2. The French laboratory at Chooz will provide all suitable skilled technicians labor necessary for installation.
3. All M&S estimates are free of overhead costs, consistent with the regulations of the participating universities.
4. Estimated effort rates are fully burdened with respect to the listed institution.
5. No overtime rates are assumed for the duration of the project.
6. The effort cost listed for each task refers to the incurred costs which are over and above the base operating funding supplied by the DOE. Argonne National Laboratory has agreed to support 25% of the cost of all Argonne effort from base funding.
7. All costs are listed in FY05 dollars. No escalation has been applied.

Detailed cost estimates are attached in a separate document. They are organized according to the WBS and are listed for each third level task. Additional details such as specific component costs, written quotes, catalog pricing, and detailed drawings are available. Each estimate is listed with a notation showing its source:

**Vendor Quote:** a written or emailed estimate for an item or system supplied within the last 3 months.

**Catalog Price:** Prices for commercially available products or services obtained from currently valid catalogs or web-based quotations.

**Shop Quote:** Supplied by a university or laboratory based shop within the last 3 months. Includes all effort, tooling and equipment.

**Engineer Estimate:** Consists of a detailed design and cost estimate provided by an engineer with previous experience with the specified system. Drawings, design assumptions and calculations are supplied where appropriate.

**Physicist Estimate:** Consists of a design and cost provided by a physicist with previous experience with the specified or similar system. These estimates are usually scaled from previously completed successful projects.

Contingency costs have been included to cover uncertainties which may result from unforeseen and unpredictable conditions or from uncertainties within the defined scope. Each level 3 element of the WBS has been assigned a contingency based on the engineer's judgment as to the solidity of the estimate and scope definition. Generally, solid quotes were given 10% contingency. It is understood that many of the catalog prices are more likely to afford cost savings as the un-explored economies of scale become available at time of purchase. Most labor and travel estimations were given a 50% contingency except in circumstances where an experienced engineer had total control of the definition of the work and scope.

### 3.4.1 Project Construction Schedule

The CHOOZ-US project schedule has been developed after consultation with the European collaborators. It is intended to mesh with the activities and schedules described in the Double-CHOOZ-LOI[4]. The specified schedule has data taking beginning at the far detector in early 2007 with the near detector coming on line at the beginning of 2008. We therefore assume that the CHOOZ-US project will continue uninterrupted over the 3 years from July 2005 to July 2008 and that sufficient funds will be provided. With that in mind, a short description of the schedule for each task follows:

**1.3 PMTs** - The production of PMTs has the longest timescale for the project. The order will therefore be placed immediately on funding of the project. We expect to receive the order in 2 batches one in each of the first two years of the project. Checkout and testing of the PMTs will proceed with availability. The operating voltage will be determined during these tests at Louisiana State University. Installation of the PMTs will occur around the end of 2006 for the far detector and in the fall of 2007 for the near detector.

**2.2 Outer Veto** - The outer veto will not need to be available until the near detector installation. As a result, the first year will primarily be spent in design and prototype testing. Production is expected to begin in spring 2006 and last until the fall of 2007. Final installation at the experimental location is expected at the end of 2007.

**3.1 Analog Front End Electronics** - The electronics designs and prototype testing will be completed by early 2006 when final production can begin. The electronics system will be shipped

to the experiment and tested by early 2007 for availability during the far detector startup. The front-end electronics task at Drexel University will use existing graduate student RA and travel support at approximately 2/3 FTE level, as the Drexel group makes the transition from KamLAND to Double-CHOOZ over the next two years, however some additional operations funding is included here as necessary for the Double-CHOOZ effort.

**3.4 High Voltage** - The high voltage system design is almost complete and uses mostly commercially available components. Procurement of the components and checkout will happen by the middle of 2006 and installation at the experiment will be completed by the end of that year.

**3.5 Slow Control and Monitoring** - The slow control and PMT rate monitoring systems will both go through design and production by July 2006. They will then be shipped to the experiment and be available for the testing and use by early 2007.

**4.2 Mechanical Deployment of Sources in 3-dimensions** - The calibration deployment system will complete its design phase by the end of 2005. This will allow production to begin rapidly so that it can be assembled in conjunction with the main inner detector in France. This will be completed for the far detector by fall of 2006 and for the near detector by the middle of 2007.

**4.3 Laser System** - The laser calibration system requires only commercially available components which will be shipped directly to the experimental location. The purchase order will be submitted in 2006 such that delivery, installation and checkout can be performed by the middle of 2007.

**Management and Common Projects** - Management of individual projects and the integration and coordination with the European collaborators will be a continuous process during the life of the project. The transportation of US components to the experimental location is expected to occur in 3 shipments. These shipments are loosely expected to occur in fall 2006, spring 2007 and fall 2007.

On the basis of the preceding schedule considerations, the required funding, including contingency, is shown in Table 14. The plan to start this project in the summer of 2005 will utilize forward funding from two of the Universities.

## 3.5 Project Management

The CHOOZ-US management plan is driven by several priorities:

- The project is a partnership between several Universities and Argonne National Laboratory. The latter should provide Project Management and Engineering Support to the CHOOZ-US group. It is crucial that the group management be aware of the needs and capabilities of both types of institution to ensure project success.
- The detector systems in the U.S. project scope must be interfaced with other detector systems being designed and constructed by groups in Europe. To avoid confusion and potential technical conflicts, there must be clear and consistent coordination among all collaborators.



Table 14: CHOOZ-US Cost Profile. The costs are shown for each major task over the expected 3 years of the project (defined from July 1 2005 to June 30 2008). The listed costs are in FY05 dollars and contain the contingencies described in the detailed budget description.

WBS	Description	Year 1	Year 2	Year 3	Totals
1.3	PMTs	\$1,050,553	\$1,056,705	\$7,801	\$2,115,060
2.2	Outer Veto	\$509,414	\$595,755	\$213,909	\$1,319,079
3.1	Front End Electronics	\$4,500	\$264,525	\$0	\$269,025
3.4	High Voltage	\$402,689	\$16,065	\$0	\$418,755
3.5	Slow Control/Monitoring	\$74,135	\$18,824	\$0	\$92,959
4.2	Calibration Deployment	\$151,096	\$88,082	\$0	\$239,178
4.3	Laser System	\$0	\$55,031	\$0	\$55,031
5.	Management/Common Projects	\$110,025	\$122,818	\$116,421	\$349,265
Totals		\$2,302,413	\$2,217,809	\$338,133	\$4,858,356

- A quick measurement of  $\theta_{13}$  is top priority of Double-CHOOZ. This necessitates beginning immediately on the design and specification of detector systems, especially for long lead time items such as PMTs. To make this feasible we must forward-fund these efforts through the universities. It is crucial that these funds are used in the most effective way for all U.S. detector subsystems and not just those in the scope of the universities providing the forward funding.
- Each institution has a stake in providing operating funds for detector construction and it is crucial that a coherent plan is developed for coordination of the operating fund requests from the various U.S. groups.

The organization structure is shown in Figure 20. The Double-CHOOZ Spokesperson is Herve de Kerret from APC and PCC College de France who has overall responsibility for Double-CHOOZ. The CHOOZ-US collaboration will operate as an integral part of the Double-CHOOZ, but for reporting and management purposes, a CHOOZ-US structure will be maintained. The principal investigator from each institution in the U.S. will be a member of the Institutional Committee, which has the responsibility of electing the US co-spokespersons. To coordinate laboratory and university efforts the Institutional Committee is initially electing two US Co-Spokespersons. Maury Goodman is a physicist at Argonne National Laboratory and a recognized leader on the Soudan 2 experiment. He was also spokesman for P-822, the original proposal for a long-baseline neutrino beam at Fermilab. Professor Robert Svoboda is a senior professor at Louisiana State University and was Co-Convener for Solar Neutrinos on the Super-Kamiokande experiment and University Coordinator for the construction of the KamLAND detector. They will carry overall responsibility for all technical and budgetary aspects of CHOOZ-US contributions. They will also be responsible for coordinating the overall project with the European collaborators and will report to the host country spokesperson on the overall progress of the U.S. construction effort. In the remainder of this section, the co-spokespersons will refer only to CHOOZ-US.

Reporting to the Co-Spokespersons on the technical coordination of the detector construction project is the Project Manager. Project management will be the responsibility of Argonne National

Laboratory, with Physicist Dr. David Reyna designated as the initial Project Manager. He will work with the Project Engineer to

- Develop Memoranda of Understanding (MOUs) with each institution which would be used to coordinate all spending and to spell out budget and schedule expectations.
- Track project costs and milestones toward completion of the project.
- Organize periodic reviews of the work of the university and laboratory groups in cooperation with the Department of Energy.
- Monitor the work breakdown structure and submit quarterly reports to the Department of Energy.

The two CHOOZ-US co-spokespersons together with the Project Manager have primary responsibility for communicating with the Department of Energy. The Co-spokesperson from Argonne and the Project Manager are responsible for assuring the DOE that the CHOOZ-US project is proceeding appropriately.

The Project Engineer for the project is Victor Guarino, an engineer at Argonne National Laboratory. He will serve as the point-of-contact for technical issues in coordinating with the European groups and will oversee the engineering plan for the U.S. portion of the detector, including projects in the university scope. He will work in close concert with Florence Ardellier, the designated European Project Manager from Saclay.

The project budget will be reviewed on a regular basis by a Budget Committee, which consists of the two Co-Spokespersons, US Project Manager, Project Engineer, and the PI's from the University of Tennessee (Y.Kamyshkov) and Drexel University (Charles Lane). They will make recommendations to the co-spokespersons on funding priorities and on the allocation of contingency based on the reports from the US Project Manager and inputs from all the university Principle Investigators (PI's).

At every stage of this project, including design, assembly and installation, safety will be a paramount concern. This will be done by incorporating the following principles at every stage of the project: clear management responsibilities, documentation, a working atmosphere of safety, Integrated Safety Management. A Quality Assurance plan for the project will be developed in accordance with policies and recommendations from the Department of Energy and any other appropriate agencies.

Once Double-CHOOZ is commissioned and fully operational, the US Project Manager will be replaced with an analysis structure selected by the Institutional Committee in coordination with the entire collaboration. All collaborating groups are free to participate in any of the scientific goals of Double-CHOOZ.

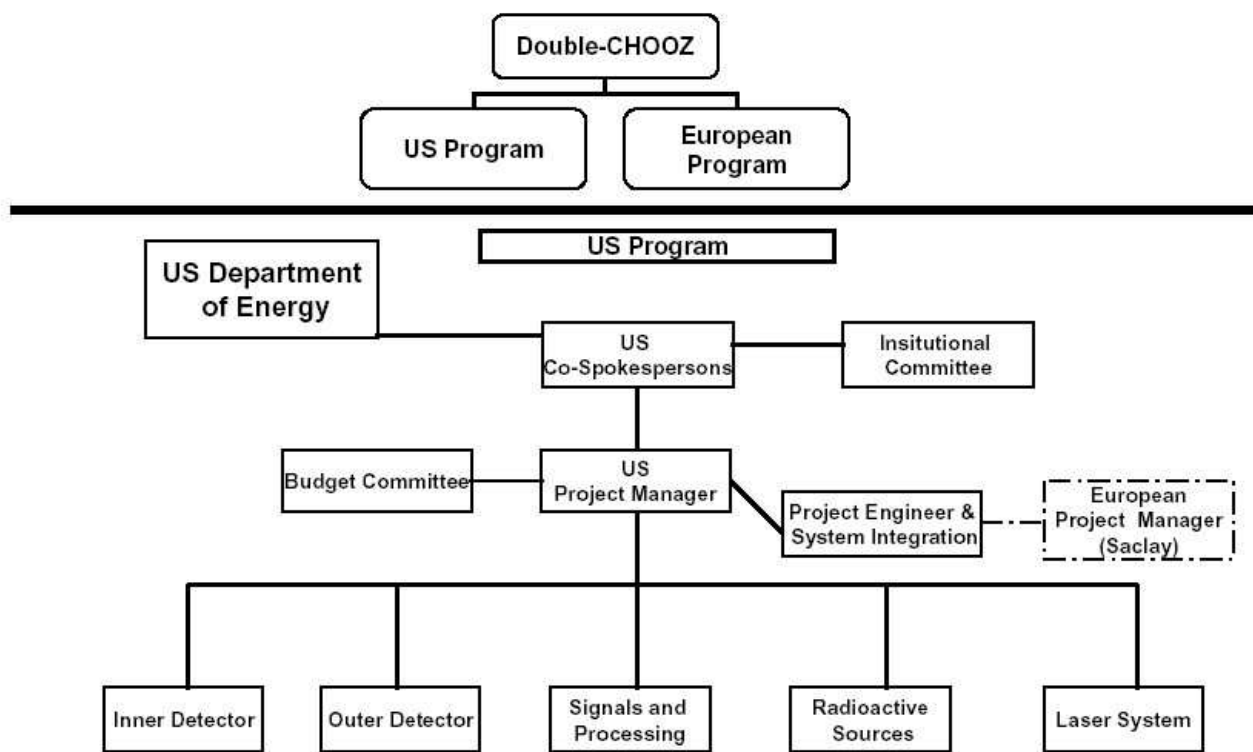


Figure 20: Proposed management structure for CHOOZ-US.

## References

- [1] The White Paper, “A New Nuclear Reactor Neutrino Experiment to Measure  $\theta_{13}$ ” is available at <http://www.hep.anl.gov/minos/reactor13/white.html>, also hep-ex/0402041
- [2] P.Huber, M.Lindner, T.Schwetz, and W.Winter, “Reactor neutrino experiments compared to superbeams”, *Nucl. Phys.*, **B** 665, 487 (2003)
- [3] H.Minakata, H.Sugiyama, O.Yasuda, K.Inoue, and F.Suekane, “Reactor measurement of  $\theta_{13}$  and its complementarity to long-baseline experiments”, *Phys. Rev* **D** 68, 033017 (2003)
- [4] F. Ardellier et al., Letter of Intent for Double-CHOOZ:  
<http://doublechooz.in2p3.fr/0405032.pdf>
- [5] Angra <http://www.hep.anl.gov/minos/reactor13/Angra/proposal.html>
- [6] Braidwood <http://mwtheta13.uchicago.edu>
- [7] Daya Bay <http://www.physics.hku.hk/events/workshops/neutrino/>
- [8] Diablo Canyon <http://theta13.lbl.gov/>
- [9] KASKA <http://neutrino.hep.sc.niigata-u.ac.jp>
- [10] M.Apollonio, *et al.*, *Eur. Phys. J.* **C**27, 331 (2003)
- [11] “The Neutrino Matrix”, APS multidivisional Neutrino Study, October 2004.
- [12] H. Minakata, H. Sugiyama, O. Yasuda, K. Inoue and F. Suekane, a hep-ph/0211111 (2002)
- [13] S.M. Bilenky, D. Nicolo and S.T. Petcov, hep-ph/0112216 (2001).
- [14] S.T. Petcov and M. Piai, hep-ph/0112074 (2001).
- [15] P. Huber, M. Lindner, T. Schwetz and W. Winter, *Nucl. Phys.* B665, 487 (2003).
- [16] M. Apollonio *et al.* (CHOOZ Collaboration), *Eur. Phys. J.* C27, 331 (2003).
- [17] F.X. Hartmann, Proc. of the 4th Int. Solar Neutrino Conference, Heidelberg, Germany, (1999).
- [18] Q. R. Ahmad *et al.* (SNO Collaboration), *Phys. Rev. Lett.* 89, 011301 (2002).
- [19] (Palo Verde Collaboration) *NIM A* 385, 85-90 (1997).
- [20] S. Croft, *NIM A* 281, 103-106 (1989).
- [21] A. Dementyev *et al.*, *Nucl. Phys.* **B** (Proc. Suppl.), 70 486 (1999).
- [22] M. Ambrosio *et al.* (MACRO Collaboration), *Phys. Lett.* B434, 451 (1998).
- [23] G. Alimonti *et al.* (BOREXINO Collaboration), *Astropart. Phys.* 8, 141 (1998).
- [24] T. Hagner, R. von Hentig, B. Heisinger, L. Oberauer, S. Schönert, F. von Feilitzsch and E. Nolte, *Astropart. Phys.* 14, 33 (2000).

- [25] G. Horton-Smith, J. Atwell, R.D. McKeown, P Vogel, Presentation at the Workshop on Future Low Energy Neutrino Experiments, Technical University Munich, Munich, 9-11 October (2003).
- [26] B. Achkar *et al.*, Phys. Lett. B **374**, 243 (1996).
- [27] Garciaz, Ph.D. thesis, University of Provence (1992).
- [28] K. Eguchi *et al.*, (KamLAND Collaboration), Phys. Rev. Lett. **90**, 021802 (2003).
- [29] S. M. Barr and I. Dorsner, Nucl. Phys. B **585**, 79 (2000) [arXiv:hep-ph/0003058].
- [30] Guido Altarelli and Ferruccio Feruglio. Theoretical models of neutrino masses and mixings. 2002.
- [31] R. Barbieri, T. Hambye and A. Romanino, JHEP **0303**, 017 (2003) [arXiv:hep-ph/0302118].
- [32] M. C. Chen and K. T. Mahanthappa, arXiv:hep-ph/0305088.
- [33] H. S. Goh, R. N. Mohapatra and S. P. Ng, hep-ph/0308197.
- [34] T. Asaka, W. Buchmuller and L. Covi, Phys. Lett. B **563**, 209 (2003) [arXiv:hep-ph/0304142].
- [35] K. S. Babu, J. C. Pati and F. Wilczek, Nucl. Phys. B **566**, 33 (2000) [arXiv:hep-ph/9812538].
- [36] T. Blazek, S. Raby and K. Tobe, Phys. Rev. D **62**, 055001 (2000) [arXiv:hep-ph/9912482].
- [37] R. Kitano and Y. Mimura, Phys. Rev. D **63**, 016008 (2001) [arXiv:hep-ph/0008269].
- [38] C. H. Albright and S. M. Barr, Phys. Rev. D **64**, 073010 (2001) [arXiv:hep-ph/0104294].
- [39] N. Maekawa, Prog. Theor. Phys. **106**, 401 (2001) [arXiv:hep-ph/0104200].
- [40] G. G. Ross and L. Velasco-Sevilla, Nucl. Phys. B **653**, 3 (2003) [arXiv:hep-ph/0208218].
- [41] M. C. Chen and K. T. Mahanthappa, Phys. Rev. D **68**, 017301 (2003) [arXiv:hep-ph/0212375].
- [42] S. Raby, Phys. Lett. B **561**, 119 (2003) [arXiv:hep-ph/0302027].
- [43] W. Buchmuller and D. Wyler, Phys. Lett. B **521**, 291 (2001) [arXiv:hep-ph/0108216].
- [44] M. Bando and M. Obara, Prog. Theor. Phys. **109**, 995 (2003) [arXiv:hep-ph/0302034].
- [45] W. Grimus and L. Lavoura, JHEP **0107**, 045 (2001) [arXiv:hep-ph/0105212].
- [46] W. Grimus and L. Lavoura, Phys. Lett. B **572**, 189 (2003) [arXiv:hep-ph/0305046].
- [47] K. S. Babu, E. Ma and J. W. F. Valle, Phys. Lett. B **552**, 207 (2003) [arXiv:hep-ph/0206292].
- [48] R. Kuchimanchi and R. N. Mohapatra, Phys. Lett. B **552**, 198 (2003) [arXiv:hep-ph/0207373].
- [49] T. Ohlsson and G. Seidl, Nucl. Phys. B **643**, 247 (2002) [arXiv:hep-ph/0206087].
- [50] S. F. King and G. G. Ross, Phys. Lett. B **574**, 239 (2003) [arXiv:hep-ph/0307190].

- [51] M. Honda, S. Kaneko and M. Tanimoto, JHEP **0309**, 028 (2003) [arXiv:hep-ph/0303227].
- [52] R. F. Lebed and D. R. Martin, arXiv:hep-ph/0312219.
- [53] M. Bando, S. Kaneko, M. Obara and M. Tanimoto, arXiv:hep-ph/0309310.
- [54] A. Ibarra and G. G. Ross, Phys. Lett. B **575**, 279 (2003) [arXiv:hep-ph/0307051].
- [55] T. Appelquist and R. Shrock, Phys. Lett. B **548**, 204 (2002) [arXiv:hep-ph/0204141].
- [56] T. Appelquist, M. Piai, and R. Shrock, Phys. Rev. D, in press [arXiv:hep-ph/0308061].
- [57] P. H. Frampton, S. L. Glashow and T. Yanagida, Phys. Lett. B **548**, 119 (2002) [arXiv:hep-ph/0208157].
- [58] J.-w. Mei and Z.-z. Xing, arXiv:hep-ph/0312167.
- [59] Andre de Gouvea and Hitoshi Murayama. Statistical test of anarchy. 2003.
- [60] R. N. Mohapatra, M. K. Parida and G. Rajasekaran, arXiv:hep-ph/0301234.
- [61] The latest SK analyses have been reported at HEP2003 and NOON04.
- [62] W. P. Oliver *et al.*, Nucl. Instrum. Meth. A **276**, 371 (1989).
- [63] <http://www.maxim-ic.com/1-Wire.cfm>
- [64] <http://www.ibutton.com/weather/>
- [65] <http://www.sunnuclear.com/products/radon/radon.asp>
- [66] F. Ardellier, *et al.*, “Letter of Intent for Double-CHOOZ”, chapter 7, arXiv:hep-ex/0305032, May, 2004.
- [67] International Critical Tables of Numerical Data, Physics, Chemistry and Technology (1st Electronic Edition), Edited by: Washburn, E.W. 1926-1930; 2003, Knovel. <http://www.knovel.com/knovel2/Toc.jsp?BookID=735>.
- [68] A. Turkevich, *et al.*, Proceedings of the National Academy of Sciences of the United States of America **94** (15): 7807-7810, July 22, 1997. R. Gurriaran R, *et al.*, Journal of Environmental Radioactivity **72** (1-2): 137-144 2004.
- [69] P. Cauwels, J. Buysse, A. Poffijn, G. Eggermont, Radiation Physics and Chemistry **61** (3-6): 649-651, June 2001.
- [70] SNO Collaboration (J. Boger, *et al.*), Nucl.Instrum.Meth. A**449** (2000) 172-207.
- [71] North Central Regional publication 393, Kansas State University, October, 1991; <http://www.oznet.ksu.edu/library/hlsaf2/ncr393.pdf>. See also U.S. Code of Federal Regulations chapter 29, 1910.1000, Table Z-1, “Limits for Air Contaminants”.

## A The U.S. Collaboration

The signers of this proposal have extensive experience in reactor neutrino experiments: CHOOZ (Lane), Palo Verde (Busenitz) and KamLAND (Bugg, Busenitz, Dazeley, Efremenko, Horton-Smith, Kamyshev, Lane, and Svoboda). There is also experience in a wide variety of other neutrino experiments including IMB (LoSecco and Svoboda), Soudan 2 (Goodman), MACRO (Lane), SNO (Kutter), MINOS (Goodman and Reyna), Brookhaven 704 (LoSecco), LSND (Stancu and Metcalf), MiniBooNE (Stancu and Metcalf), Fermilab E1A (LoSecco), Fermilab E594 (Goodman) and Super-Kamiokande (Dazeley and Svoboda).

## B The Full Collaboration

F. Ardellier<sup>5</sup>, I. Barabanov<sup>10</sup>, J.C. Barrière<sup>5</sup>, M. Bauer<sup>7</sup>, S. Berridge<sup>20</sup>, L. Bezrukov<sup>10</sup>, Ch. Buck<sup>13</sup>, W. Bugg<sup>20</sup>, J. Busenitz<sup>1</sup>, C. Cattadori<sup>8,9</sup>, B. Courty<sup>2,15</sup>, M. Cribier<sup>2,5</sup>, F. Dalnoki-Veress<sup>13</sup>, N. Danilov<sup>4</sup>, S. Dazeley<sup>12</sup>, H. de Kerret<sup>2,15</sup>, A. Di Vacri<sup>8,19</sup>, G. Drake<sup>3</sup>, Y. Efremenko<sup>20</sup>, A. Etenko<sup>16</sup>, M. Fallot<sup>17</sup>, Ch. Grieb<sup>18</sup>, M. Goeger<sup>18</sup>, M. Goodman<sup>3</sup>, J. Grudzinski<sup>3</sup>, V. Guarino<sup>3</sup>, A. Guertin<sup>17</sup>, G. Horton-Smith<sup>11</sup>, C. Hagner<sup>21</sup>, W. Hampel<sup>13</sup>, F.X. Hartmann<sup>13</sup>, P. Huber<sup>18</sup>, J. Jochum<sup>7</sup>, Y. Kamyshev<sup>20</sup>, T. Kirchner<sup>17</sup>, Y.S. Krylov<sup>4</sup>, D. Kryn<sup>2,15</sup>, T. Kutter<sup>12</sup>, T. Lachenmaier<sup>18</sup>, C. Lane<sup>c</sup>, Th. Lasserre<sup>2,5</sup>, Ch. Lendvai<sup>18</sup>, A. Letourneau<sup>5</sup>, M. Lindner<sup>18</sup>, J. LoSecco<sup>14</sup>, F. Marie<sup>5</sup>, J. Martino<sup>17</sup>, R. McNeil<sup>12</sup>, G. Mention<sup>2,15</sup>, W. Metcalf<sup>12</sup>, A. Milsztajn<sup>5</sup>, J.P. Meyer<sup>5</sup>, D. Motta<sup>13</sup>, L. Oberauer<sup>18</sup>, M. Obolensky<sup>2,15</sup>, L. Pandola<sup>8,19</sup>, W. Potzel<sup>18</sup>, D. Reyna<sup>3</sup>, S. Schönert<sup>13</sup>, U. Schwan<sup>13</sup>, T. Schwetz<sup>18</sup>, S. Scholl<sup>7</sup>, L. Scola<sup>5</sup>, M. Skorokhvatov<sup>16</sup>, I. Stancu<sup>1</sup>, S. Sukhotin<sup>15,16</sup>, R. Svoboda<sup>12</sup>, R. Talaga<sup>3</sup>, D. Vignaud<sup>2,15</sup>, F. von Feilitzsch<sup>18</sup>, W. Winter<sup>18</sup>, E. Yanovich<sup>10</sup>

<sup>1</sup> University of Alabama, Tuscaloosa, Alabama 35487-0324, USA

<sup>2</sup> APC, 11 place Marcelin Berthelot, 75005 Paris, France

<sup>3</sup> Argonne National Lab, Argonne, IL 60439-4815, USA

<sup>4</sup> IPC of RAS, 31, Leninsky prospect, Moscow 117312, Russia

<sup>5</sup> DAPNIA (SEDI, SIS, SPhN, SPP), CEA/Saclay, 91191 Gif-sur-Yvette, France

<sup>6</sup> Drexel University, Philadelphia, Pennsylvania 19104, USA

<sup>7</sup> Eberhard Karls Universität, Wilhelmstr. D-72074 Tübingen, Germany

<sup>8</sup> INFN, LGNS, I-67010 Assergi (AQ), Italy

<sup>9</sup> INFN Milano, Via Celoria 16, 20133 Milano, Italy

<sup>10</sup> INR of RAS, 7a, 60th October Anniversary prospect, Moscow 117312, Russia

<sup>11</sup> Kansas State University, Manhattan Kansas 66506-26031, USA

<sup>12</sup> Louisiana State University, Baton Rouge, Louisiana 70803-4001, USA

<sup>13</sup> MPI für Kernphysik, Saupfercheckweg 1, D-69117 Heidelberg, Germany

<sup>14</sup> University of Notre Dame, South Bend, Indiana 46556, USA

<sup>15</sup> PCC Collège de France, 11 place Marcelin Berthelot, 75005 Paris, France

<sup>16</sup> RRC Kurchatov Institute, 123182 Moscow, Kurchatov sq. 1, Russia

<sup>17</sup> Subatech (Ecole des Mines), 4, rue Alfred Kastler, 44307 Nantes, France

<sup>18</sup> TU München. James-Franck-Str., D-85748 Garching, Germany

<sup>19</sup> University of L'Aquila, Via Vetoio 1, I-67010 Coppito, L'Aquila, Italy

<sup>20</sup> University of Tennessee, Knoxville, Tennessee 37996-1200, USA

<sup>21</sup> Universität Hamburg, Luruper Chaussee 149, D-22761 Hamburg, Germany